TPR-00-05

Nuclear Enhanced Higher-Twist Effects in the Drell-Yan Process

R. J. Fries, A. Schäfer, E. Stein

Institut für Theoretische Physik , Universität Regensburg, D-93040 Regensburg, Germany

and

B. Müller

Department of Physics, Duke University, Box 90305, Durham, North Carolina 27708-0305

Abstract: We calculate the Drell-Yan cross section, resolving the full kinematics of the lepton pair, at high transverse momentum for hadron nucleus collisions. We use the general framework of Luo, Qiu and Sterman to calculate double scattering contributions that are of twist-4 and demonstrate their nuclear enhancement. By comparing single and double scattering at RHIC energies we find that double scattering gives contributions of comparable size. We also show that the angular dependence of the Drell-Yan pair discriminates between the various double scattering contributions.

PACS numbers: 25.75.-q, 12.38.Bx, 13.85.Qk

Keywords: QCD, Structure Functions, Power Corrections, Nuclear effects

1 Introduction

In recent times the interest in understanding hard processes involving nuclei, like electron nucleus collisions ($e + A$) and hadron nucleus collisions ($h + A$), has rapidly increased. The relativistic heavy ion collider (RHIC) will provide a new tool for experimental studies of $h + A$ and $A + A$ physics. This experimental advance provides a challenge to theorists for developing a description of such reactions strictly in terms of the underlying fundamental field theory, i.e. quantum chromodynamics (QCD).

The usual way to proceed in QCD is to use factorization theorems [1] that permit a rigorous treatment of hard processes. In this approach, incalculable soft contributions are factorized into universal, process independent distribution functions. Measurement of the distribution functions in one process then allows the prediction of cross sections for other processes. An example is the Drell-Yan (DY) process where two hadrons scatter to produce a lepton pair of large invariant mass Q^2. If Q^2 is large enough the factorization theorems state, that the inclusive Drell Yan cross section can be expressed as the product of a calculable hard part and universal twist-2 parton distribution functions that can be measured, for instance in deeply inelastic lepton nucleon scattering. Such universal distribution functions have been successfully extracted from existing data. The natural question arises how this picture is changed for hadron-nucleus collisions. Differences between the twist-2 distribution of a single nucleon and those of a nucleus of mass number $A > 1$ were first discovered by the European Muon Collaboration. This phenomenon is known as the EMC effect at large values of the Bjorken scaling variable x and as shadowing at lower values of x [2].

However, strong interaction dynamics cannot solely be described in terms of twist-2 structure functions. These functions are simple one-particle correlators and have the interpretation of a probability to find a parton in the hadron with certain momentum fraction x. These distribution functions are measured when the hard probe scatters off a single parton in the nucleon. Of course, the probe may scatter off more than one parton in the target. Such processes are related to multi-parton correlators and describe corrections to the single-parton scattering process. In general they are suppressed by powers of the large scale, and are called contributions of higher twist.

If we consider processes involving large nuclei it is quite obvious that multiple scattering will be enhanced and even dominate in the limit $A \to \infty$. The classical example for enhancement of multiple scattering in $h + A$ processes is the Cronin effect, i.e. the anomalous A-dependence of the Drell-Yan cross section at large values of the transverse momentum of the lepton pair [3]. Instead of a scaling of the cross section with the volume $\sim A$ as expected in the twist-2 case, one observes an A-dependence parametrized by $\sigma^{h+A} = A^{\alpha}\sigma^{h+p}$ with $\alpha \approx 4/3$ [4]. This is a clear signal for multiple scattering and shows that higher-twist multiple scattering is grossly enhanced at large momentum transfer.

The literature contains a wide variety of approaches dealing with multiple scattering, see e.g. [5], but a rigorous formulation in the language of perturbative QCD was attempted only recently. In a series of papers, Luo, Qiu and Sterman (LQS) and recently also Guo, showed how to extend the factorization theorem beyond leading twist to get a handle on double scattering in terms of perturbative QCD [6, 7]. Their twist-4 matrix elements are correlators of two partons in the nucleus and can describe scattering off partons from different nucleons. This approach predicts a stronger dependence on the size of the nucleus than the linear scaling with A of single scattering. LQS argue that — due to the geometrical structure of the matrix elements — some of these twist-4 nuclear matrix elements pick up an additional factor $A^{1/3}$, compensating for some of the inherent suppression of higher twist corrections. This nuclear enhancement is able to describe the observed scaling with $A^{4/3}$ in certain kinematical regions.

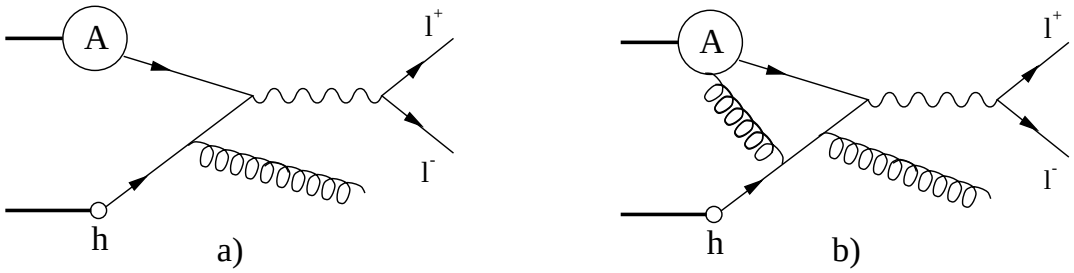

Figure 1: Single- (a) and double-scattering (b) schematically for a hadron h colliding with a nucleus A producing a $\mu^+\mu^-$ pair. One additional unobserved parton is radiated in the leading contribution to high transverse momentum $q_\perp$.

In this paper we discuss nuclear enhanced double scattering contributions to DY pair production off nuclear targets

$$h(P_2) + A(P_1 A) \longrightarrow l^+ l^- + X \tag{1}$$

in the framework of the LQS approach. It was already shown some time ago by Guo [8, 9] that higher-twist effects in the process (1) are enhanced at large transverse momentum. Extending the calculations of Guo [8], we have calculated the full kinematical dependence of the cross section $\mathrm{d}\sigma/\mathrm{d}Q^2\,\mathrm{d}q_\perp^2\,\mathrm{d}y\,\mathrm{d}\Omega$ including the angular distribution of the lepton pair and evaluated it, in particular, for $p + A$ scattering at RHIC. Our most important results were already published as a letter [10]. In this contribution we present the complete analytical results together with a brief review of the LQS approach and some technical details. We also give some numerical results not contained in [10] and an extended discussion. We will argue that nuclear enhanced double scattering corrections cannot be neglected at RHIC.

In Fig. 1 we show typical Feynman diagrams contributing to the DY process. Single scattering means that, e.g., a quark from the single hadron and an antiquark from the nucleus annihilate into a virtual photon in a hard process. To obtain large transverse momentum an additional unobserved parton, here a gluon, has always to be radiated. Double scattering in our example implies that the quark can pick up an additional gluon from the nucleus. The generalized twist-4 factorization theorem of LQS states that two distinct scattering reactions occur for double scattering. One is referred to as double-hard (DH) scattering. Here the parton from the single hadron undergoes two subsequent independent hard scattering reactions in the target. The other one is called soft-hard (SH) scattering. Here the parton from the single hadron interacts with the collective soft gluon field in the nucleus (it can e.g. be thought of as feeling the color-magnetic Lorentz force) before producing the virtual photon via the final hard scattering. At large transverse momentum interference of these two mechanisms can be neglected.

The double-hard reaction resembles the classical double scattering picture, while soft-hard scattering may have an analogy in plasma physics, where a hard scattering event can be accompanied by initial- or final-state interaction with the mean field. The first process might be accounted for by event generators in simulations of heavy-ion reactions whereas the implementation of soft-hard scattering has yet to be formulated in a fully consistent manner (see [11] for a conceptual discussion).

It would be helpful to find observables with vanishing or at least very small contributions from single scattering. The measurement of such observables would permit the identification of twist-4 effects at larger values of Q^2 where perturbation theory is more reliable and thus provide a clearer evidence for the occurrence of double scattering. We find these observables in the angular distribution of DY pairs, namely the helicity amplitude W_Δ and the Lam-Tung relation

$W_{\Delta\Delta} = W_{\rm L}/2$ [12], both introduced in section 2. The Lam-Tung relation is analogous to the Callan-Gross relation in deep-inelastic electron nucleon scattering (DIS). Furthermore it would be helpful to find observables where double-hard and soft-hard contributions can be disentangled. These can also be found in the angular distribution of DY pairs. While SH scattering leads to non-trivial angular patterns, DH scattering does not. Any anomalous A-dependent angular distribution therefore would be a clear sign of non trivial twist-4 correlations.

Although we will focus on $h + A$ collisions, our work has been primarily motivated by the fact that higher-twist effects or multiple scattering should be most prominent in nucleus-nucleus $(A + A)$ collisions at high energy, as they will be routinely studied at RHIC. Two microscopic, QCD-inspired descriptions of nucleus-nucleus collisions at RHIC energies and beyond have been proposed in recent years. In one, the parton cascade picture [13, 14, 15], the collision is modeled as a sequence of incoherent binary scattering events among partons ("minijets"), which can be cast in a probabilistic formulation as a multiple scattering process. In the other one, the random mean-field model [16] the collision is described as a nonlinear interaction among coherent color fields carried by the colliding nuclei. We hope that the study of the interplay between soft-hard and multiple-hard processes in a simpler framework, such as $h + A$ interactions, will help to elucidate the competition between these processes in $A + A$ collisions.

The determination of multiparton correlation functions in nuclei is also an important step towards the application of QCD to nuclear physics in general. The generic enhancement of higher-twist effects in reactions involving nuclei facilitates their extraction and give the chance for a deeper theoretical understanding. They encode the essential aspects of the difference in the quark-gluon structure between isolated nucleons and nuclei. From the practical point of view a better understanding of such medium effects is necessary to be able to interpret the so called "hard probes" of high-energy heavy-ion collisions in a convincing manner.

The unintegrated Drell-Yan cross section is actually the classic example for a typical two-scale process. Both Q^2 and $q_\perp$, the mass and transverse momentum of the photon, are detected. The perturbative treatment then gives rise to logs of the type $\log^2(Q^2/q_\perp^2)$ which can become large if the scales differ substantially. In such a case they have to be resummed. Resumming large logs in the presence of additional soft gluons contained in the twist-4 correlators is a delicate task that could not be solved yet. We therefore follow a less ambitious procedure and require that both scales are of the same order, thus reducing the original two-scale problem to an effective one-scale problem. In addition the LQS formalism in its present form requires $q_\perp^2$ to be not much smaller than Q^2 in order to neglect interference terms that are not calculated up to now and which would introduce additional twist-4 matrix elements. Recently Guo, Qiu and Zhang proposed a method to describe the region of low transverse momentum and how to match it to the perturbative calculation at high $q_\perp$ [17].

Finally we would like to comment on the experimental situation. There exist data for angular coefficients on $\pi + A$ scattering, e.g. from the NA10 [18] and E615 [19] experiments which are not yet completely understood in terms of conventional QCD-treatment. These experiments measure pair masses $Q \approx 4 \ldots 8.5$ GeV and transverse momenta $q_\perp < 3$ GeV which is certainly at the limit of where we could still trust our calculation. We will focus on future RHIC perspectives where we could hopefully reach higher transverse momenta.

The paper is organized as follows: In section 2 we give the general definition of the Drell-Yan kinematics, we introduce our observables — helicity amplitudes and angular coefficients — and explain possible choices of the photon rest frame. In section 3 we remind the reader of the known twist-2 results for the helicity amplitudes. Section 4 is devoted to the calculation of the double-scattering contribution. We explain some essential features of the factorization procedure of LQS. In particular we discuss the distinction between double-hard and soft-hard scattering

and give an introduction of how to calculate them practically. Finally section 5 contains our numerical results along with a discussion and we close with a summary of our final conclusions. In the appendices we have collected some technical details referred to in the text.

2 General Definitions

2.1 Kinematics

Let a nucleus with momentum P_1^μ per nucleon collide with a hadron with momentum P_2^μ. We study lepton pair decay of virtual photons with momentum q^μ and mass $Q^2 = q^2$. In the hadron center-of-mass (c.m.) frame we take

$$P_1^\mu = \frac{1}{2}(\sqrt{S}, 0, 0, \sqrt{S}), \quad P_2^\mu = \frac{1}{2}(\sqrt{S}, 0, 0, -\sqrt{S}) \tag{2}$$

where $\sqrt{S}$ is the total center-of-mass energy. The differential cross section for Drell-Yan pair production is then given by

$$d\sigma = \frac{\alpha_{em}^2}{2SQ^4} L_{\mu\nu} W^{\mu\nu} \frac{\mathrm{d}^4 q}{(2\pi)^4} \mathrm{d}\Omega. \tag{3}$$

The solid angle Ω is parametrized by the polar and azimuthal angles θ and ϕ of one decay lepton in the rest frame of the virtual photon. We have the freedom to choose the axes in the photon rest frame conveniently. We will discuss this point after eq. (16).

The hadronic tensor follows the standard definition and is given by

$$W_{\mu\nu} = \int \mathrm{d}^4 x \, e^{iq\cdot x} \left\langle P_1 P_2 \right| j_\mu(x) j_\nu(0) \left| P_1 P_2 \right\rangle \ . \tag{4}$$

The leptonic tensor is

$$L^{\mu\nu} = 2\left(l_1^\mu l_2^\nu + l_2^\mu l_1^\nu\right) - g^{\mu\nu} Q^2 \ , \tag{5}$$

where l_1 and l_2 are the momenta of the leptons.

We rewrite the q-dependence of the cross section in terms of rapidity y, transverse momentum $q_\perp$ and mass Q of the virtual photon in the hadron c.m. frame. Introducing the hadronic Mandelstam invariants

$$\begin{aligned} S &= (P_1 + P_2)^2 \\ T &= (P_1 - q)^2 \\ U &= (P_2 - q)^2 \end{aligned} \tag{6}$$

the rapidity y of the photon is

$$y = \frac{1}{2} \ln\left(\frac{q^0 + q^3}{q^0 - q^3}\right) = \frac{1}{2} \ln\left(\frac{Q^2 - U}{Q^2 - T}\right) \ . \tag{7}$$

Likewise we can express the transverse momentum of the lepton pair in the hadron c.m. system by

$$q_\perp^2 = \frac{(Q^2 - U)(Q^2 - T)}{S} - Q^2 \ . \tag{8}$$

and we can rewrite the differential cross section as:

$$\frac{\mathrm{d}\sigma}{\mathrm{d}Q^2 \, \mathrm{d}q_\perp^2 \, \mathrm{d}y \, \mathrm{d}\Omega} = \frac{\alpha_{em}^2 \pi}{4SQ^4} L_{\mu\nu} W^{\mu\nu} \frac{1}{(2\pi)^4} \tag{9}$$

2.2 Helicity amplitudes and their frame dependence

To discuss the angular distribution of the lepton pair it is convenient to introduce helicity amplitudes $W_{\sigma,\sigma'}$ defined as

$$W_{\sigma,\sigma'} = \epsilon_\mu^{(\sigma)} \epsilon_\nu^{(\sigma')*} W^{\mu\nu} \tag{10}$$

where $\epsilon_\mu^{(\sigma)}$, $\sigma \in \{\pm 1, 0\}$ is a set of polarization vectors of the virtual photon with respect to the axes defined by the spatial unit vectors $\mathbf{X}$, $\mathbf{Y}$, $\mathbf{Z}$ in its rest frame:

$$\varepsilon_\mu^{(\pm)} = \frac{1}{\sqrt{2}}(\mp X - iY)_\mu, \qquad \varepsilon_\mu^{(0)} = Z_\mu \tag{11}$$

Following [20] it is advantageous to introduce a complete set of structure functions

$$\begin{aligned} W_{\mathrm{T}} &= W_{1,1} \\ W_{\mathrm{L}} &= W_{0,0} \\ W_{\Delta} &= \frac{1}{\sqrt{2}} \left(W_{1,0} + W_{0,1} \right) \\ W_{\Delta\Delta} &= W_{1,-1} \end{aligned} \tag{12}$$

which are referred to as the transverse, longitudinal, spin flip, and double spin flip helicity amplitudes. Due to parity conservation other combinations are related to these by $W_{\sigma,\sigma'} = (-)^{\sigma+\sigma'} W_{-\sigma,-\sigma'}$. In terms of these helicity structure functions the cross section can be written as

$$\begin{aligned} \frac{\mathrm{d}\sigma}{\mathrm{d}Q^2\, \mathrm{d}q_\perp^2\, \mathrm{d}y\, \mathrm{d}\Omega} &= \frac{\alpha_{em}^2}{64\pi^3 S Q^2} \\ &\left(W_{\mathrm{TL}} \left(1 + \cos^2\theta\right) + W_{\mathrm{L}} \left(\frac{1}{2} - \frac{3}{2} \cos^2\theta \right) + W_{\Delta} \left(\sin 2\theta \cos\phi \right) + W_{\Delta\Delta} \left(\sin^2\theta \cos 2\phi \right) \right). \end{aligned} \tag{13}$$

The angular dependence can be integrated out which reduces the cross section to

$$\frac{\mathrm{d}\sigma}{\mathrm{d}Q^2\, \mathrm{d}q_\perp^2\, \mathrm{d}y} = \frac{\alpha_{em}^2}{64\pi^3 S Q^2} \left(\frac{16}{3}\pi \right) W_{\mathrm{TL}} \tag{14}$$

with $W_{\mathrm{TL}} = W_{\mathrm{T}} + \frac{1}{2} W_{\mathrm{L}} = -\frac{1}{2} W_\mu^\mu$. The ratio of the angular dependent and angular integrated cross sections is usually parametrized in two standard forms [18, 21]:

$$\begin{aligned} \frac{16\pi}{3} \left(\frac{\frac{\mathrm{d}\sigma}{\mathrm{d}Q^2\, \mathrm{d}q_\perp^2\, \mathrm{d}y\, \mathrm{d}\Omega}}{\frac{\mathrm{d}\sigma}{\mathrm{d}Q^2\, \mathrm{d}q_\perp^2\, \mathrm{d}y}} \right) &= (1 + \cos^2\theta) + A_0 \left(\frac{1}{2} - \frac{3}{2} \cos^2\theta \right) + A_1 \sin 2\theta\, \cos\phi + \frac{A_2}{2} \sin^2\theta\, \cos 2\phi = \\ &= \frac{4}{\lambda + 3} \left(1 + \lambda \cos^2\theta + \mu \sin 2\theta\, \cos\phi + \frac{\nu}{2} \sin^2\theta\, \cos 2\phi \right) \end{aligned} \tag{15}$$

in terms of two sets of angular coefficients

$$A_0 = \frac{W_{\mathrm{L}}}{W_{\mathrm{TL}}} \qquad A_1 = \frac{W_{\Delta}}{W_{\mathrm{TL}}} \qquad A_2 = \frac{2\, W_{\Delta\Delta}}{W_{\mathrm{TL}}}, \tag{16}$$

$$\lambda = \frac{2 - 3A_0}{2 + A_0} \qquad \mu = \frac{2A_1}{2 + A_0} \qquad \nu = \frac{2A_2}{2 + A_0}. \tag{17}$$

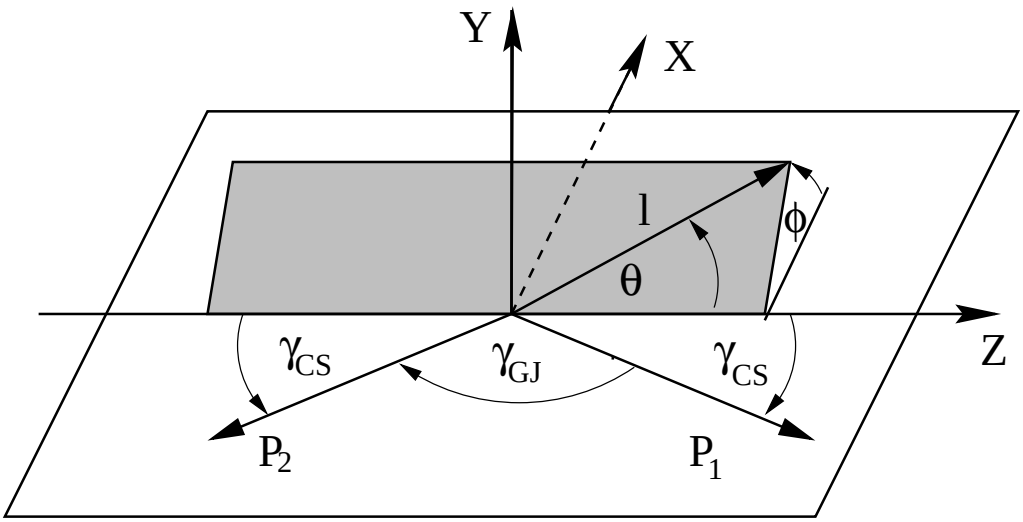

Figure 2: Definition of the angles θ and ϕ in the rest frame of the lepton-pair. The frame shown here is the Collins-Soper frame.

At this point it is necessary to comment on the proper choice of coordinate axes in the photon rest system with respect to which the polar and azimuthal angles θ and ϕ are defined. Clearly the helicity amplitudes and angular coefficients depend on the chosen frame. Two prominent examples are the Collins-Soper frame (CS) and the Gottfried-Jackson frame (GJ) which are discussed in detail in [20]. When we boost from the hadron c.m. frame to a lepton c.m. frame, the collinearity of the hadron momenta $\mathbf{P}_1$ and $\mathbf{P}_2$ is lost and they span a plane which we identify with the **X**-**Z**-plane. We are still free to fix **Z** within this plane. In the Collins-Soper frame we choose **Z** to bisect the angle between $\mathbf{P}_1$ and $-\mathbf{P}_2$, see Fig. 2. The angle between **Z** and $\mathbf{P}_1$ and between **Z** and $-\mathbf{P}_2$ is called $\gamma_{\rm CS}$ In the Gottfried-Jackson frame **Z** lies in the direction of $\mathbf{P}_1$. We have introduced the the angle $\gamma_{\rm GJ}$ between $\mathbf{P}_1$ and $\mathbf{P}_2$ for short notations in that case. Obviously we have $2\gamma_{\rm CS}+\gamma_{\rm GJ}=\pi$. See Appendix 7.1 for more details. Also note that for $q_\perp = 0$ both frames are equal and ϕ is no longer defined.

In order to obtain the results in both frames in a straightforward way we use the projectors given by Mirkes [22]

$$
\begin{aligned}
P^{\mu\nu}_{\rm TL} &= -g^{\mu\nu} & P^{\mu\nu}_{\rm L1} &= \frac{P_1^\mu P_1^\nu}{E_1^2} \\
P^{\mu\nu}_{\rm L12} &= \frac{P_1^\mu P_2^\nu + P_2^\mu P_1^\nu}{E_1 E_2} & P^{\mu\nu}_{\rm L2} &= \frac{P_2^\mu P_2^\nu}{E_2^2}
\end{aligned}
\tag{18}
$$

where E_1 and E_2 are the energies of the hadrons in the lepton c.m. frame. In terms of hadronic Mandelstam variables and the photon momentum these are

$$
E_1 = \frac{Q^2-T}{2Q} = \frac{e^{-y}}{2Q}\sqrt{S(Q^2+q_\perp^2)}, \qquad E_2 = \frac{Q^2-U}{2Q} = \frac{e^{y}}{2Q}\sqrt{S(Q^2+q_\perp^2)}. \tag{19}
$$

Contracting the hadronic tensor with these projectors gives amplitudes $T_\alpha = P^{\mu\nu}_\alpha W_{\mu\nu}$, $\alpha \in \{\mathrm{TL}, \mathrm{L1}, \mathrm{L2}, \mathrm{L12}\}$ which are just linear combinations of the helicity amplitudes in the different frames. These can be found by linear transformations

$$
\begin{pmatrix} W^{(\beta)}_{\rm TL} \\ W^{(\beta)}_{\rm L} \\ W^{(\beta)}_{\Delta} \\ W^{(\beta)}_{\Delta\Delta} \end{pmatrix} = M_{(\beta)} \begin{pmatrix} T_{\rm TL} \\ T_{\rm L}1 \\ T_{\rm L}2 \\ T_{\rm L}12 \end{pmatrix}, \tag{20}
$$

with $\beta \in \{\mathrm{CS}, \mathrm{GJ}\}$. The transformation matrices $M_{(\beta)}$ follow from simple geometry and are given in Appendix 7.1 for the CS and GJ frames.

3 Leading twist results

To make this paper self contained we give the leading order results for the angular coefficients. Due to twist-2 factorization the hadronic tensor is given by a convolution of a perturbatively calculable partonic tensor and two twist-2 distribution functions:

$$W_{\mu\nu} = g^2 e_q^2 \sum_{a,b} \int \frac{\mathrm{d}\xi_1}{\xi_1} \int \frac{\mathrm{d}\xi_2}{\xi_2} H_{\mu\nu}^{a+b}(\xi_1, \xi_2) f_{a/A}(\xi_1) f_{b/h}(\xi_2) 2\pi\delta(s+t+u-Q^2). \tag{21}$$

The sum runs over partons a and b in the nucleus A and the single hadron h respectively and ξ_1, ξ_2 are their momentum fractions. We denote the strong coupling by g and e_q is the fractional electric charge of the quark flavour coupling to the virtual photon. The $f(\xi)$ correspond to twist-2 parton distribution functions defined in the usual way as

$$\begin{aligned} f_{q/h}(\xi) &= \frac{1}{P^+} \int \frac{\mathrm{d}y^-}{2\pi} P^+ e^{i\xi P^+ y^-} \, \frac{1}{2} \langle P | \, \bar{q}(0) \gamma^+ \mathcal{P} q(y^-) \, | P \rangle \\ f_{g/h}(\xi) &= \frac{1}{\xi P^+} \int \frac{\mathrm{d}y^-}{2\pi} e^{i\xi P^+ y^-} \, \langle P | \, F_a^{+\nu}(0) \mathcal{P} F_{a\,\nu}{}^{+}(y^-) \, | P \rangle \end{aligned} \tag{22}$$

for quarks and gluons, respectively in a hadron moving with momentum P^+ along the light cone [1]. q and F denote quark fields and gluon field strength tensors and $\mathcal{P}$ is the path-ordered exponential

$$\mathcal{P} = P \exp\left\{ ig \int_{y^-}^{0} \mathrm{d}x^- A^+(x^-) \right\} \tag{23}$$

which makes the definition gauge invariant. In the following we will not write this path-ordered exponential explicitly, but it is assumed to be inserted between all factors in a product of operators referring to different space-time points. In the $A^+ = 0$ gauge this term will disappear but we will always use covariant gauge. Note that we also suppressed the dependence of the distribution function on the factorization scale μ^2.

The partonic tensor $H_{\mu\nu}^{a+b}$ represents the hard part of the process. We have introduced partonic Mandelstam variables by

$$\begin{aligned} s &= (\xi_1 P_1 + \xi_2 P_2)^2 = \xi_1 \xi_2 S \\ t &= (\xi_1 P_1 - q)^2 = \xi_1 (T - Q^2) + Q^2 \\ u &= (\xi_2 P_2 - q)^2 = \xi_2 (U - Q^2) + Q^2. \end{aligned} \tag{24}$$

The δ-function in eq. (21) stems from the on-shell condition for the unobserved emitted parton with momentum l. It can be used for trivial integration of ξ_2 via

$$\delta(l^2) = \delta(s+t+u-Q^2) = \frac{1}{\xi_1 S + U - Q^2} \delta\left(\xi_2 + \frac{Q^2 + \xi_1 (T - Q^2)}{\xi_1 S + U - Q^2} \right). \tag{25}$$

We can decompose the partonic tensor in a way completely analogous to the decomposition of the hadronic tensor $W_{\mu\nu}$ in terms of helicity amplitudes. Therefore we define the four projections

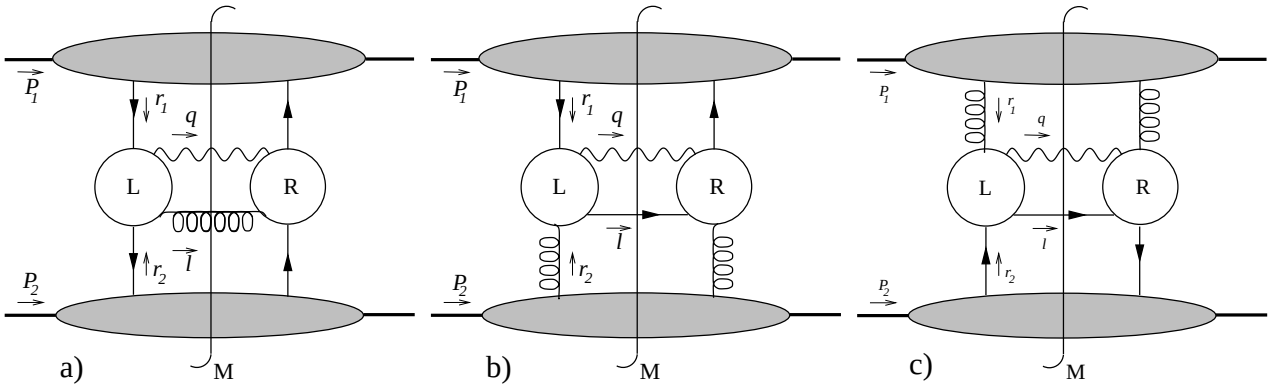

Figure 3: Twist-2 contributions to order α_s: annihilation (a), and Compton processes (b and c). The blobs L and R stand for all possible tree-level diagrams.

$H_{\rm TL}^{a+b}, H_{\rm L}^{a+b}, H_{\Delta}^{a+b}, H_{\Delta\Delta}^{a+b}$ which are obtained in the same way as in eqs. (10,12). This allows us to write hadronic tensor and helicity amplitudes as

$$W_\alpha = 8\pi^2\alpha_s e_q^2 \sum_{a,b} \int_B^1 \frac{{\rm d}\xi_1}{\xi_1} \frac{1}{\xi_1(Q^2-T)-Q^2} f_{a/A}(\xi_1) f_{b/h}(\bar{\xi}_2) H_\alpha^{a+b}(\xi_1,\bar{\xi}_2). \tag{26}$$

with $B = \frac{-U}{S+T-Q^2}$, $\bar{\xi}_2 = -\frac{Q^2+\xi_1(T-Q^2)}{\xi_1 S+U-Q^2}$, $\alpha_s = g^2/4\pi$ and $\alpha \in \{\mu\nu, TL, L, \Delta, \Delta\Delta\}$. There are three kinds of partonic processes contributing to the leading-twist process at large transverse momentum: quark-antiquark annihilation ($\bar{q}+q$) and Compton processes with a gluon from the single hadron ($q+g$) or the nucleus ($g+q$). They are shown in Fig. 3.

The cross section for the leading twist DY pair production at large transverse momentum is well-known [22, 23]. For completeness we give the results in the Collins-Soper frame in Appendix 7.2. The relation $H_{\Delta\Delta} = \frac{1}{2}H_{\rm L}$ is precisely the so-called Lam-Tung relation [12]. It can be expressed in terms of angular coefficients as $A_0 = A_2$ or $2\nu - (1-\lambda) = 0$. This relation holds for all partonic subprocesses and is not specific for the Collins-Soper frame but holds in any photon rest frame as long as the **Z**-axis lies in the reaction plane. Corrections arise at next-to-leading order (NLO) [22]. Note that H_Δ^{a+b} picks up an additional sign compared with H_Δ^{b+a} in contrast to the other helicity amplitudes. This is due to the inversion of the orientation of the angle $\gamma_{\rm CS}$ if we interchange the roles of P_1 and P_2. For symmetric collisions, e. g. $p+p$, this leads to the leading-twist result $W_\Delta = 0$.

4 Twist-4 Factorisation

4.1 Soft-hard and double-hard scattering

For the calculation of the double scattering contributions we use the approach of Luo, Qiu and Sterman which is presented e. g. in [6, 8]. We consider it worthwile to repeat some aspects here. In Fig. 4 we illustrate the forward diagrams that need to be calculated for double scattering. The box denotes all possible partonic subprocesses. We have to introduce a cut to obtain the corresponding hadronic tensors. This is not only possible in the middle but we also have to include interference graphs which appear if the forward diagram is cut in an asymmetrical way. In Fig. 5 we give concrete examples for graphs which involve a quark-gluon matrix element in the nucleus and an antiquark coming from the single hadron. The first diagram is cut in the middle (M), the others are cut left (L) and right (R).

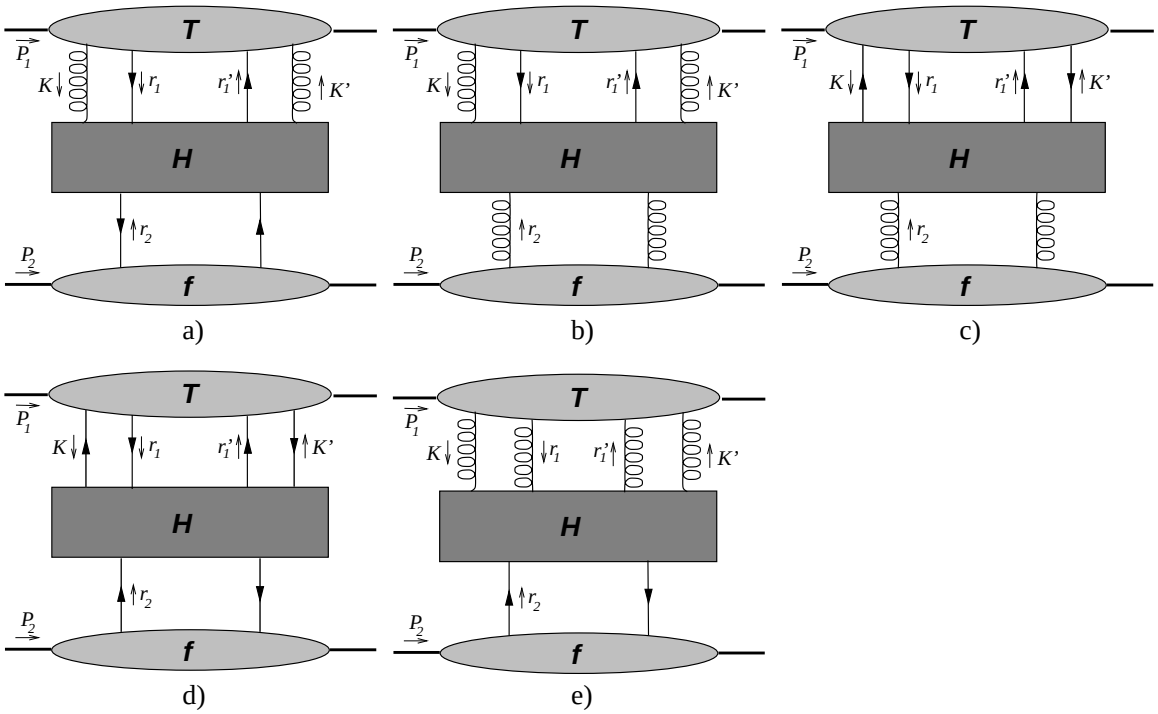

Figure 4: Collection of the schematic forward processes we want to consider for double scattering. Factorization allows separate treatment of twist-4 and twist-2 matrix elements (T and f) and hard part (H).

The starting point for the calculation of the hadronic tensor is the forward scattering amplitude in fourth order of the strong coupling constant g:

$$T_{\mu\nu} = \frac{g^4 e_q^2}{4!} \int \mathrm{d}^4x\, \mathrm{d}^4x_1\, \mathrm{d}^4x_2\, \mathrm{d}^4x_3\, \mathrm{d}x_4 e^{iqx} \left\langle P_1P_2\right| T \left[J_\rho(x_3) J_\alpha(x_1) j_\mu(0) j_\nu(x) \right. \\ \left. J_\beta(x_2) J_\sigma(x_4) A^\rho(x_3) A^\alpha(x_1) A^\beta(x_2) A^\sigma(x_4) + \dots \right] \left|P_1P_2\right\rangle \tag{27}$$

where j (J) are electromagnetic (color) quark currents and A denotes gluon fields. T is the time-ordering operator. Dots indicate further contributions involving more gluon fields with gluon self interaction and less quark currents such that the power of g remains four. By application of Wick's theorem we obtain all diagrams which potentially contribute to the forward process.

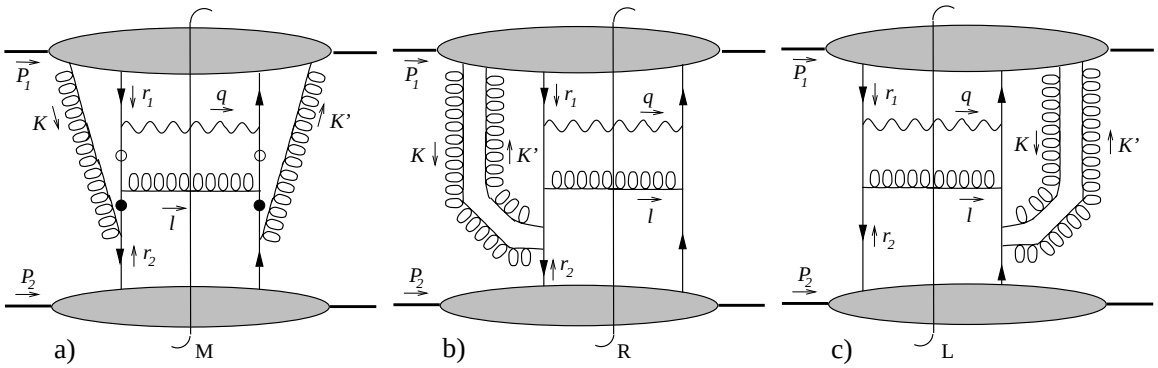

Figure 5: Examples for double-scattering diagrams with the partonic process $qg + \bar{q}$ cut in the middle (a), right (b) and left (c). Circles in Fig. (a) indicate poles from propagators which lead to finite gluon momentum (open) or soft gluon momentum (filled).

We classify diagrams by their partonic subprocess $ab + c$ where a and b are partons from the nucleus and c comes from the single hadron. Our notation for the parton momenta is shown in Fig. 4. We concentrate first on $qg + \bar{q}$ which can be realized e.g. by the diagrams of Fig. 5. As a first step towards factorization we perform Fierz transformations in color and Dirac space for the fermion lines entering and leaving the blobs:

$$q^i_\alpha(0)\bar{q}^j_\beta(z) = -\frac{1}{4}\left(\gamma_\mu\right)_{\alpha\beta}\bar{q}^{j'}(z)\gamma^\mu q^{i'}(0)\left(\frac{1}{N_c}\delta_{j'i'}\delta_{ij} + 2t^A_{j'i'}t^A_{ij}\right) + \dots . \tag{28}$$

Here the t^A are the $SU(N_c)$ Gell-Mann matrices, and N_c is the number of colors. Latin characters are color indices, greek one are Dirac indices. We keep only Dirac structures which give leading contributions to the unpolarized Drell-Yan process. After Fourier transformations of the fields we end up with

$$\begin{aligned} T^{qg+\bar{q}}_{\mu\nu} = \int \frac{\mathrm{d}^4 l}{(2\pi)^4}\frac{\mathrm{d}^4 r_1}{(2\pi)^4}\frac{\mathrm{d}^4 r_2}{(2\pi)^4}\frac{\mathrm{d}^4 K}{(2\pi)^4}\frac{\mathrm{d}^4 K'}{(2\pi)^4}\int \mathrm{d}^4 y\,\mathrm{d}^4 z_1\,\mathrm{d}^4 z_3\,\mathrm{d}^4 z_4 \\ (2\pi)^4\delta^{(4)}(r_1 + r_2 + K - l - q)e^{ir_1 z_1}e^{-ir_2 y}e^{iKz_3}e^{-iK'z_4}\frac{1}{2}\left\langle P_1\right|\bar{q}(0)\gamma^\eta q(z_1)A^\rho(z_3)A^\sigma(z_4)\left|P_1\right\rangle \\ \left(-\frac{1}{2}\right)\left\langle P_2\right|\bar{q}(0)\gamma^\tau q(y)\left|P_2\right\rangle e_q^2 g^4\frac{1}{N_c^2}\frac{\delta^{RS}}{N_c^2-1}\sum_d S(d)^{RS}_{\nu\sigma\tau\rho\mu\eta}. \end{aligned} \tag{29}$$

We used the fact that forward matrix elements only depend on the relative coordinates. So, after shifting positions in each matrix element separately, we introduced a new set of space-time coordinates (y,z_1,z_3,z_4). l is the momentum of the unobserved radiated parton. The index d runs over all diagrams of the class $qg + \bar{q}$ and $S(d)^{RS}_{\rho\mu\epsilon\nu\sigma\tau}$ contains all perturbative propagators and vertices of the hard part of diagram d, with γ_η (γ_τ) inserted for the upper (lower) blob, and traces over color and Dirac indices. For the diagram of Fig. 5(a) we have e. g.

$$\begin{aligned} S^{RS}_{\nu\sigma\tau\rho\mu\eta} = \frac{1}{4}\,\mathrm{Tr}\left[(-i\gamma_\nu)\frac{i(\not r_1 + \not K - \not K' - \not q)}{(r_1 + K - K' - q)^2 + i\epsilon}(-i\gamma_\beta t^B)\frac{i(-\not r_2 - \not K')}{(r_2 + K')^2 + i\epsilon}(-i\gamma_\sigma t^S)\right. \\ \left.\gamma_\tau(-i\gamma_\rho t^R)\frac{i(-\not r_2 - \not K)}{(r_2 + K)^2 + i\epsilon}(-i\gamma_\alpha t^A)\frac{i(\not r_1 - \not q)}{(r_1 - q)^2 + i\epsilon}(-i\gamma_\mu)\gamma_\eta\right]\frac{i(-g^{\alpha\beta})\delta^{AB}}{l^2 + i\epsilon}. \end{aligned} \tag{30}$$

R and S are color indices of gluon fields. Note that we have coupled quark and gluon field operators in the nuclear matrix elements separately to color singlets. We have omitted a term proportional to $(d^{RES} + if^{RES})\left\langle P_1\right|\bar{q}\gamma^\eta t^E q A^{R\rho}A^{S\sigma}\left|P_1\right\rangle$ which would induce color forces between quark and gluon in the nucleus. This would not allow to factorize quarks and gluons in color space to test the size of the nucleus. Such contributions are not expected to show nuclear enhancement, i.e. scaling by $A^{4/3}$.

Next we perform the light cone expansion, i.e. we use that the partons move almost collinear to the hadron in the infinite momentum frame. We introduce the parton momentum fractions by setting $r_1 = \xi_1 P_1$, $r_2 = \xi_2 P_2$, $K = xP_1 + K_\perp$ and $K' = x'P_1 + K'_\perp$. $r'_1 = r_1 + K - K'$ is fixed by momentum conservation in the upper forward matrix element. Note that we have to allow one parton (called b here) from the nucleus to be soft with essentially zero longitudinal momentum. Therefore we must take into account transverse momenta $K_\perp$ and $K'_\perp$ to get a contribution in higher orders of the collinear expansion as we will see later. Now one can integrate the trivial degrees of freedom in eq. (29). To complete the factorization we perform a Sudakov decomposition of the γ-matrices in the forward matrix elements on the light cone and retain only the leading terms $\gamma^\eta = \frac{P_1^\eta}{P_1^+}\gamma^+$, $\gamma^\tau = \frac{P_2^\tau}{P_2^-}\gamma^-$. Then we can introduce twist-2 distribution

functions $f_{c/h}(\xi_2)$, given in eq. (22), for the lower blob. Finally we cut the forward diagram. This sets the radiated unobserved parton with momentum l on the mass shell and in the hard part all expressions right to the cut receive a complex conjugation.

Hence after these first steps we have factorized the hadronic tensor in a straightforward way. We get

$$W_{\mu\nu}^{ab+c} = (4\pi\alpha_s)^2 e_q^2 \int \frac{\mathrm{d}\xi_1}{\xi_1}\frac{\mathrm{d}\xi_2}{\xi_2}\,\mathrm{d}x P_1^+\,\mathrm{d}^2K_\perp\,\mathrm{d}x' P_1^+\,\mathrm{d}^2K'_\perp f_{c/h}(\xi_2)(2\pi)\delta(l^2) \\ \bar{T}_{ab}(\xi_1, x, x', K_\perp, K'_\perp)\bar{H}_{\mu\nu}^{ab+c}(\xi_1, \xi_2, x, x', K_\perp, K'_\perp). \tag{31}$$

We have derived eq. 31 for our examples of Fig. 5, but this equation holds for all processes shown in Fig.4. We have separated the soft part involving the twist-2 distribution function $f_{c/h}$ and the nuclear matrix element $\bar{T}_{ab}$ from the hard part $\bar{H}_{\mu\nu}^{ab+c}$.

For our example $qg + \bar{q}$ we are left with a quark-gluon matrix element in the nucleus

$$\bar{T}_{qg}(\xi_1, x, x', K_\perp, K'_\perp) = \int \frac{\mathrm{d}z_1^-}{2\pi}\frac{\mathrm{d}z_3^-\,\mathrm{d}^2z_3^\perp}{(2\pi)^3}\frac{\mathrm{d}z_4^-\,\mathrm{d}^2z_4^\perp}{(2\pi)^3} e^{ir_1^+z_1^-} e^{iK^+z_3^-} e^{-iK_\perp z_3^\perp} e^{-iK'^+z_4^-} e^{iK'_\perp z_4^\perp} \\ \frac{1}{2}\langle P_1|\,\bar{q}(0)\gamma^+ q(z_1^-)A^\rho(z_3^-, z_3^\perp)A^\sigma(z_4^-, z_4^\perp)\,|P_1\rangle\,. \tag{32}$$

For other classes of processes we also need the quark-quark and gluon-gluon correlators $\bar{T}_{gg}$ and $\bar{T}_{qq}$ which are given by eq. (32) with the second line replaced by

$$\frac{1}{\xi_1 P_1^+}\langle P_1|\,F^{\omega+}(0)F^+_\omega(z_1^-)A^\rho(z_1^-, z_1^\perp)A^\sigma(z_4^-, z_4^\perp)\,|P_1\rangle \quad \text{for } \bar{T}_{gg} \\ \frac{1}{2}\langle P_1|\,\bar{q}(0)\gamma^+ q(z_1^-)\bar{q}(z_3^-, z_3^\perp)\gamma^\kappa q(z_4^-, z_4^\perp)\,|P_1\rangle \quad \text{for } \bar{T}_{qq}. \tag{33}$$

Again here the field operators of each single parton form color singlets separately. We have arranged the first two field operators referring to the nuclear parton a in the way they appear in the corresponding twist-2 structure function while the remaining two field operators of parton b are still in their original form.

The hard part for the $qg + \bar{q}$-process is

$$\bar{H}_{\mu\nu}^{qg+\bar{q}}(\xi_1, \xi_2, x, x', K_\perp, K'_\perp) = \frac{1}{N_c^2}\frac{1}{N_c^2 - 1}(-g^{\alpha\beta})r_1^\eta r_2^\tau \frac{1}{4}\sum_d S(d)^{RR}_{\nu\sigma\tau\rho\mu\eta}\Big|_{\text{cut}}. \tag{34}$$

Hard parts for other processes are obtained analogously. The delta function in eq. (31) can be rewritten for the cases in which the diagrams are cut in the middle (M), right (R) or left (L) as

$$\begin{aligned} (\mathrm{M}): \quad \delta(l^2) &= (\xi_2 S + T - Q^2)^{-1}\delta(\xi_1 + x - \tilde{\xi}_b) \\ (\mathrm{R}): \quad \delta(l^2) &= (\xi_2 S + T - Q^2)^{-1}\delta(\xi_1 + x - x' - \xi_c) \\ (\mathrm{L}): \quad \delta(l^2) &= (\xi_2 S + T - Q^2)^{-1}\delta(\xi_1 - \xi_c) \end{aligned} \tag{35}$$

where

$$\tilde{\xi}_b = -\frac{\xi_2(U - Q^2) + Q^2 - 2qK_\perp + K_\perp^2}{\xi_2 S + T - Q^2} \qquad \text{and} \qquad \tilde{\xi}_c = \tilde{\xi}_b\big|_{K_\perp = 0}. \tag{36}$$

As pointed out in various papers [7, 8] there are in principle two contributions to double scattering: There can be two hard scattering reactions of the parton c from the single hadron

or the outgoing unobserved parton on one side and partons a and b from the nucleus on the other side. This is called double-hard scattering. Furthermore there can occur processes where the parton c from the single hadron or the outgoing parton picks up one soft nuclear parton b in addition to one hard scattering off the nuclear parton a. This is called soft-hard scattering. These are not only qualitative notions but they can be rigorously derived from the equations given above. One can understand them in terms of poles in the hard part of the scattering tensor. In eq. (31) we have four momentum integrations $\mathrm{d}\xi_1\,\mathrm{d}\xi_2\,\mathrm{d}x\,\mathrm{d}x'$ and four propagators. We will perform the ξ_1-integration by making use of the delta function $\delta(l^2)$. The propagators provide poles with respect to x and x'. In general we expect two poles in x and two poles in x'. Application of the residue theorem will fix the momenta and it is easy to check that two poles give large momenta $x = x_{\mathrm{hard}} = x'$, respectively and the other ones give small momenta $x = x_{\mathrm{soft}} = x'$ with $x_{\mathrm{hard}} \gg x_{\mathrm{soft}} \ll 1$ as long as $q_\perp \sim Q$.

To be more precise the pole structure we expect for our example in Fig. 5(a) is

$$W_{\mu\nu} \sim \int \mathrm{d}x \frac{L(x)}{(x - x_{\mathrm{soft}} + i\epsilon)(x - x_{\mathrm{hard}} + i\epsilon)} \int \mathrm{d}x' \frac{R(x')}{(x' - x_{\mathrm{soft}} - i\epsilon)(x' - x_{\mathrm{hard}} - i\epsilon)}, \tag{37}$$

where L and R stand for the numerators of the amplitudes left and right of the cut depending on x and x'. The residue theorem implies

$$W_{\mu\nu} \sim \left[\frac{L(x = x_{\mathrm{soft}})}{x_{\mathrm{soft}} - x_{\mathrm{hard}}} - \frac{L(x = x_{\mathrm{hard}})}{x_{\mathrm{soft}} - x_{\mathrm{hard}}}\right] \left[\frac{R(x' = x_{\mathrm{soft}})}{x_{\mathrm{soft}} - x_{\mathrm{hard}}} - \frac{R(x' = x_{\mathrm{hard}})}{x_{\mathrm{soft}} - x_{\mathrm{hard}}}\right] \tag{38}$$

Soft-hard and double-hard scattering correspond to the quadratic terms proportional to $L(x = x_{\mathrm{soft}})R(x' = x_{\mathrm{soft}})$ and $L(x = x_{\mathrm{hard}})R(x' = x_{\mathrm{hard}})$ respectively. We follow the arguments of reference [7, 8] and neglect the remaining mixed terms of eq. (38) which are interference terms between soft and hard rescattering. This is permitted if $q_\perp$ is not too small. In the case $q_\perp^2 \ll Q^2$ however we obtain $x_{\mathrm{soft}} \approx x_{\mathrm{hard}}$. The interference will then be important and eventually spoil nuclear enhancement due to the negative signs in eq. (38) [8]. Since the integrated Drell-Yan cross section does not exhibit nuclear enhancement, we even expect a suppression effect at low values of transverse momenta [9].

Most diagrams we naively get from Wick's theorem for double scattering show a different behaviour. For them the propagators do not provide four but only three or two poles — but at least one in each variable x and x'. This implies that only soft-hard, only double-hard or neither of these contributions can occur. For example it is easy to understand from this analysis that only symmetrically (M) cut diagrams can contribute to double-hard scattering. Consider the diagram of Fig. 5(b). The propagator on the right-hand side has denominator $[(r_1' - q)^2 - i\epsilon]$, from which x and x' dependences cancel out. On the left-hand side, the propagator at the bottom of the diagram contributes a denominator $(r_2 + K)^2 + i\epsilon = \xi_2 S(x + \frac{K_\perp^2}{\xi_2 S} + i\epsilon)$. This is a soft pole which fixes x to $x_{\mathrm{soft}} = -\frac{K_\perp^2}{\xi_2 S} \ll 1$. The remaining two propagators on the left-hand side fix x' to either a soft or a hard value. Therefore we have two contributions: (i) $x = x'$ is small. This means that parton b is soft — in Fig. 5(b) this is the gluon from the nucleus. Together with the production of the virtual photon which is always a hard process, this constitutes a soft-hard double scattering process. (ii) x is soft and x' is hard. This is what we called a soft-hard interference because parton b has different momenta on the left and the right side of the diagram, i.e. momentum is transferred between partons a and b. We omit this contribution as explained above. We conclude that there is no double-hard scattering contribution from the diagram in Fig. 5(b) since x cannot be hard. On the other hand the diagram in Fig. 5(a) is an example in which all four poles occur, indicated by small circles.

We now discuss another technical point which has some relevance for nuclear enhancement. Consider again eq. (37) and the example of Fig. 6(a) and note that the numerators L and R contain exponential functions $e^{ixP_1^+ z_3^-} e^{i(\tilde{\xi}_b - x)P_1^+ z_1^-}$ and $e^{-ix'P_1^+ z_4^-}$. To apply the residue theorem we have to close the integration contours. For $z_3^- - z_1^- > 0$ we have to close the x-integration in the upper complex x-plane with no poles encircled and therefore vanishing integral. On the other hand for $z_3^- - z_1^- < 0$ we must close in the lower complex x-plane with soft and hard pole encircled. Therefore these poles always introduce additional theta functions in coordinate space, in our example $\Theta(z_1^- - z_3^-)$ from the x integration and $\Theta(-z_4^-)$ from the x' integral. The presence of these Θ functions in the matrix elements is an essential ingredient of the proof of the following rule about the cancellation of final state interactions for soft-hard scattering: If at least one soft parton from the twist-4 matrix element is directly coupled to the outgoing unobserved parton line these graphs do not contribute to soft-hard scattering. These graphs exhibit more than one possibility to set the cut and the nuclear enhancement cancels between the contributions with different cuts due to the particular arrangement of Θ-functions in that case [7].

Hence, after a careful discussion of the pole structure of each diagram the number of diagrams we are finally forced to evaluate can be reduced. Figs. 6 and 7 show the diagrams that contribute to double-hard and soft-hard scattering, respectively. We marked the poles used to fix momenta. Also we omitted soft-hard contributions with soft quarks since they should be suppressed compared to their counterparts with soft gluons.

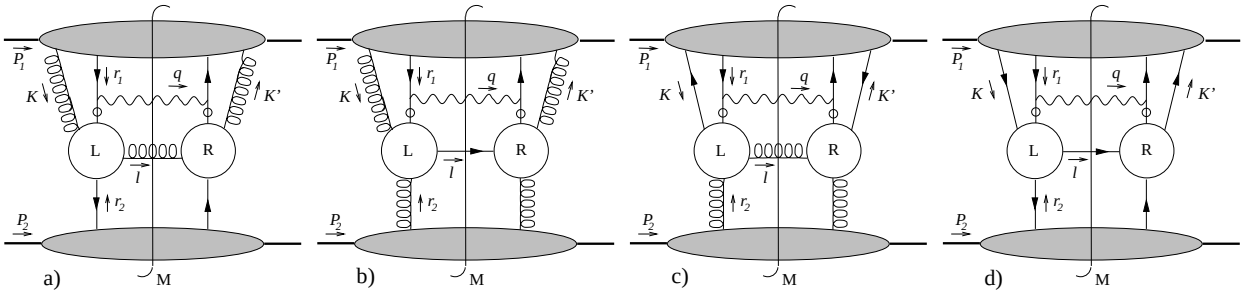

Figure 6: Graphs contributing to double-hard scattering: $qg + \bar{q}$, $qg + g$, $q\bar{q} + g$ and $qq + \bar{q}$. There are additional processes with structures similar to the last one, e.g. $q\bar{q} + q$. This is discussed in the next section. The blobs (L) and (R) stand for all possible tree-level diagramms. Propagators providing poles which are used to fix hard momenta are indicated by small open circles.

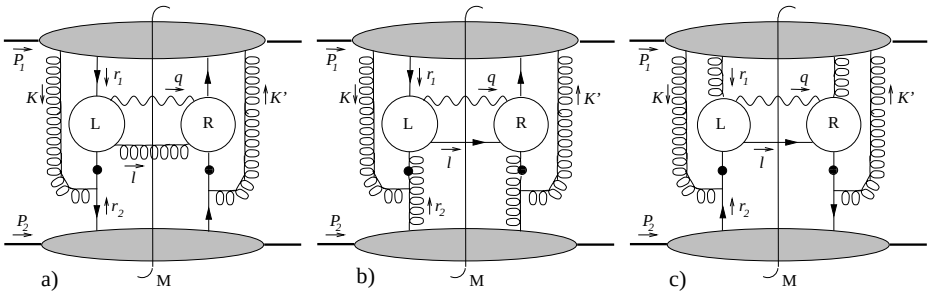

Figure 7: Graphs contributing to soft-hard scattering: $qg + \bar{q}$, $qg + g$ and $gg + q$. The blobs (L) and (R) stand for all possible tree-level diagramms. Only symmetrically cut diagrams (M) are shown. Corresponding right (R) and left (L) cut diagrams have to be added. Propagators providing poles which are used to fix soft momenta are indicated by small filled circles.

4.2 Calculation of the double-hard processes

First we investigate the case of double-hard scattering. Since all parton momenta are hard we can work in the collinear limit and set $K_\perp = 0 = K'_\perp$ immediately. We perform the integrations over x and x' only taking into account contributions from hard poles. These poles are marked with circles in Fig. 6. They fix momenta to the values $x = x_h = x'$ and $\xi_1 = x_a$ with

$$x_a = \frac{Q^2}{Q^2 - T} \tag{39}$$

$$x_h = \tilde{\xi}_a - x_a = -\frac{\xi_2(U - Q^2) + Q^2}{\xi_2 S + T - Q^2} - \frac{Q^2}{Q^2 - T} \tag{40}$$

Note that x_a is determined by kinematical variables only whereas x_h depends on the integration variable ξ_2. Two additional Θ-functions in the light cone space-time coordinates show up as explained above.

The field operators of the second parton in the nuclear matrix element are selected in such a way that we get the usual twist-2 light cone operator $\bar{q}\gamma^+ q$ for quarks and field strength tensors $F^{\omega+}F^{+}_{\ \omega}$ for gluons. In the latter case we have to turn two factors of P_1^+ into light cone derivatives $(ix_h)^{-1}\partial_{z_3^-}$, $(-ix_h)^{-1}\partial_{z_4^-}$ and perform partial integrations to let them act on the gluon fields in the matrix element. Hard gluons carry only physical polarizations, this allows us to set $\partial^+ A^\rho(z_3^-)\partial^+ A^\sigma(z_4^-) = F^{\omega+}(z_3^-)F^{+}_{\ \omega}(z_4^-)\frac{1}{2}(-g^{\rho\sigma} + \bar{n}^\rho n^\sigma + n^\rho \bar{n}^\sigma)$ with the usual light cone basis vectors $\bar{n}^\rho = P_1^\rho / P_1^+$, $\bar{n}^\rho = P_2^\rho / P_2^-$.

We are now able to give the final result for double-hard scattering. For a partonic subprocess of the type $ab + c$ we have

$$W_\alpha^{ab+c} = \frac{(2\pi)^2 (4\pi\alpha_s)^2 e_q^2}{Q^2 - T} \int_B^1 \frac{\mathrm{d}\xi_2}{\xi_2} \frac{1}{\xi_2 S + T - Q^2} f_{c/H}(\xi_2) T_{ab}^{\mathrm{DH}}(x_a, x_h) \frac{1}{x_h} H_\alpha^{\mathrm{DH}/ab+c}(x_a, x_h, \xi_2) \tag{41}$$

with $\alpha \in \{\mu\nu, TL, L, \Delta, \Delta\Delta\}$. Note that parton a is always a quark or antiquark for double-hard scattering and e_q denotes its electric charge. As in the helicity amplitudes which arise from contractions of the hadronic tensor $W_{\mu\nu}$ defined in eq. 10, here we use the same contractions for the hard partonic part $H_{\mu\nu}$, defining amplitudes H_{TL}, H_{L}, H_Δ and $H_{\Delta\Delta}$ depending on the frame. The hard parts for the relevant diagrams can be written as

$$\begin{aligned}
H_{\mu\nu}^{\mathrm{DH},qg+\bar{q}} &= \mathcal{C}\frac{1}{Q^2}\frac{1}{4}\,\mathrm{Tr}\left[(\not{x}_1 - \not{q}) R_{\sigma\beta}\ \not{x}_2 L_{\rho\alpha}(\not{x}_1 - \not{q})\gamma_\mu\ \not{x}_1\gamma_\nu\right]_{\substack{\xi_1 = x_a \\ x = x' = x_h}} \frac{1}{2}\, g^{\alpha\beta} g^{\rho\sigma} \\
H_{\mu\nu}^{\mathrm{DH},qg+g} &= \mathcal{C}\frac{1}{Q^2}\frac{1}{4}\,\mathrm{Tr}\left[(\not{x}_1 - \not{q}) R_{\sigma\beta}\ \not{l} L_{\rho\alpha}(\not{x}_1 - \not{q})\gamma_\mu\ \not{x}_1\gamma_\nu\right]_{\substack{\xi_1 = x_a \\ x = x' = x_h}} \frac{1}{2}\, g^{\alpha\beta} g^{\rho\sigma} \\
H_{\mu\nu}^{\mathrm{DH},q\bar{q}+g} &= \mathcal{C}\frac{1}{Q^2}\frac{1}{4}\,\mathrm{Tr}\left[(\not{x}_1 - \not{q}) R_{\sigma\beta}\ \not{K} L_{\rho\alpha}(\not{x}_1 - \not{q})\gamma_\mu\ \not{x}_1\gamma_\nu\right]_{\substack{\xi_1 = x_a \\ x = x' = x_h}} \frac{1}{2}\, g^{\alpha\beta} g^{\rho\sigma}.
\end{aligned} \tag{42}$$

$L_{\rho\alpha}$ and $R_{\sigma\beta}$ indicate the sum over all possible tree level diagrams for the blobs at the left and the right side of the corresponding diagram in Fig. 6. Each diagram provides an individual color factor which is indicated symbolically by the factor $\mathcal{C}$. For partonic processes with three participating fermions we have to distinguish between different possible combinations of quark and antiquarks and different flavours. In principle there are contributions written in our short notation as $q\bar{q} + q$, $q\bar{q} + \bar{q}$ and $qq + \bar{q}$. Each of these contributes four diagrams contained in Fig. 6(d). In addition, there are processes of the type $q\bar{q} + q'$, $qq' + \bar{q}$ and $qq' + \bar{q}'$, which are each represented by a single diagram. In our notation q is a quark or antiquark, $\bar{q}$ the corresponding antiparticle and q' denotes a quark or antiquark of a different flavour than q. As an example we give the hard part for the $q\bar{q} + q$ subprocess:

$$H_{\mu\nu}^{\mathrm{DH},q\bar{q}+q} = \mathcal{C}\frac{1}{Q^2}\frac{1}{8}\left\{\mathrm{Tr}\left[(\not{r}_1 - \not{q})\gamma_\sigma \not{K}\gamma_\beta(\not{r}_1 - \not{q})\gamma_\mu \not{r}_1\gamma_\nu\right]\mathrm{Tr}\left[\not{r}_2\gamma_\rho \not{l}\gamma_\alpha\right](r_1+K-q)^{-4} - \right.$$
$$- \mathrm{Tr}\left[(\not{r}_1 - \not{q})\gamma_\sigma \not{l}\gamma_\beta \not{r}_2\gamma_\rho \not{K}\gamma_\alpha(\not{r}_1 - \not{q})\gamma_\mu \not{r}_1\gamma_\nu\right](r_1+K-q)^{-2}(r_2+K)^{-2} +$$
$$\left. + (K \leftrightarrow l)\right\}_{\substack{\xi_1 = x_a \\ x = x' = x_h}} g^{\alpha\beta}g^{\rho\sigma}. \quad (43)$$

Note the relative sign that is due to the different number of fermion loops in the corresponding diagrams.

The $T_{ab}^{\mathrm{DH}}(x_a, x_h)$ are the universal nuclear matrix elements for double-hard scattering introduced in [6, 24]. They depend on the momentum fractions x_a, x_h of both hard partons from the nucleus and are given by

$$\begin{aligned}
T_{qg}^{\mathrm{DH}}(x_a,x_h) &= \frac{1}{x_h}\frac{1}{2}\int \mathrm{d}z_4^- \frac{\mathrm{d}z_3^-}{2\pi}\frac{\mathrm{d}z_1^-}{2\pi}\Theta(z_1^- - z_3^-)\Theta(-z_4^-)e^{ix_aP_1^+z_1^-}e^{ix_hP_1^+(z_3^- - z_4^-)} \\
&\quad \langle P_1|\, F^{\omega+}(z_4^-)F^+{}_\omega(z_3^-)\bar{q}(0)\gamma^+q(z_1^-)\,|P_1\rangle \\
T_{q\bar{q}}^{\mathrm{DH}}(x_a,x_h) &= -\frac{1}{4}\int \mathrm{d}z_4^- P_1^+ \frac{\mathrm{d}z_3^-}{2\pi}\frac{\mathrm{d}z_1^-}{2\pi}\Theta(z_1^- - z_3^-)\Theta(-z_4^-)e^{ix_aP_1^+z_1^-}e^{ix_hP_1^+(z_3^- - z_4^-)} \\
&\quad \langle P_1|\, \bar{q}(0)\gamma^+q(z_1^-)\bar{q}(z_3^-)\gamma^+q(z_4^-)\,|P_1\rangle \\
T_{qq}^{\mathrm{DH}}(x_a,x_h) &= \frac{1}{4}\int \mathrm{d}z_4^- P_1^+ \frac{\mathrm{d}z_3^-}{2\pi}\frac{\mathrm{d}z_1^-}{2\pi}\Theta(z_1^- - z_3^-)\Theta(-z_4^-)e^{ix_aP_1^+z_1^-}e^{ix_hP_1^+(z_3^- - z_4^-)} \\
&\quad \langle P_1|\, \bar{q}(0)\gamma^+q(z_1^-)\bar{q}(z_4^-)\gamma^+q(z_3^-)\,|P_1\rangle\,.
\end{aligned} \quad (44)$$

We are now ready to explain the origin of nuclear enhancement in these matrix elements. As mentioned above the fields of both partons are coupled separately to colour singlets. This allows to probe distances up to the diameter of a large nucleus. Each spatial integration of the matrix element arises from a Fourier transformation and we expect it to be accompanied by a rapidly oscillating exponential function (since $P_1^+ \longrightarrow \infty$). At first glance, this seems to rule out coherence over the whole nucleus. However only z_1^- and $z_3^- - z_4^-$ in eq. (44) are restricted by phase factors while $z_3^- + z_4^-$ is not. Hence, we can set $\int \mathrm{d}(z_3^- + z_4^-)$ to be proportional to the nuclear radius $R_A \approx r_0 A^{1/3}$ and obtain an additional factor of $A^{1/3}$. Here $r_0 \approx 1.1$ fm is the radius of a nucleon.

To find a reasonable model for the double-hard matrix elements imagine the insertion of a complete set of states $\sum_P |P\rangle\langle P|/(2P^+V) = 1$ where V is the volume of the nucleus. Neglecting for a moment the Θ-function and the integration over $z_3^- + z_4^-$ we can compare these definitions with the common definitions of twist-2 structure functions in eq. (22). Assuming that the sum over states is saturated by the lowest lying nucleon state double hard matrix elements reduce to a product of two twist-2 structure functions times a dimensional factor which scales like $A^{4/3}$

$$T_{ab}^{\mathrm{DH}}(x_a,x_h) = CA^{4/3}f_{a/A}(x_a)f_{b/A}(x_h). \quad (45)$$

$f_{a/A}$ is the nuclear parton distribution per nucleon in a nucleus with mass number A and proton number Z, $N = A - Z$, given by

$$f_{a/A}(x) = \frac{Z}{A}f_{a/p}(x) + \frac{N}{A}f_{a/n}(x). \quad (46)$$

In a primitive model one can simply set the remaining free integration with respect to $z_4^- + z_3^-$ equal to R_A and obtains $C = 3/(8\pi r_0^2) \approx 0.005$ GeV^2. Although the factorization of the double-hard matrix element into a product of two twist-2 distribution functions and the scaling by $A^{4/3}$ seems to provide a reasonable model, the choice of the normalization factor C is a hot matter of

discussion, see section 5. The Θ-functions provide an ordering of both single scattering events on the light cone. They simply express the fact that scattering off parton b takes place before the scattering off parton a. This corresponds to $z_4^- < 0$ on the left side and to $z_3^- < z_1^-$ on the right side of each diagram.

Now we give the final results for the hard parts. For the evaluation it is important also to include ghosts, whenever one can close gluon lines through the non-perturbative blobs. For $H_{\rm TL}^{\rm DH} = -\frac{1}{2} H^{\rm DH}{}_{\mu}{}^{\mu}$, which enters the angular integrated cross section, we reproduce the results of [8]. We have listed them in Appendix 7.3 for all subprocesses. The helicity amplitude $W_{\rm TL}$ is independent of the frame. Due to the special form of all diagrams contributing to double-hard scattering we easily see that the contractions $P_{\rm L1}^{\mu\nu} H_{\mu\nu}^{\rm DH}$ and $P_{\rm L12}^{\mu\nu} H_{\mu\nu}^{\rm DH}$ in eq. (42) always vanish, and for the last contraction we get

$$P_{\rm L2}^{\mu\nu} H_{\mu\nu}^{\rm DH} = \frac{Q^2 S\left[(Q^2-T)(Q^2-U) - Q^2 S\right]}{(Q^2-T)^2 (Q^2-U)^2} H_{\rm TL}^{\rm DH} = \frac{Q^2 q_\perp^2}{(Q^2+q_\perp^2)^2} H_{\rm TL}^{\rm DH} \tag{47}$$

for all processes. For the Collins-Soper frame this leads to the simple relations

$$W_{\rm L}^{\rm DH} = \sin^2\gamma_{\rm CS} W_{\rm TL}^{\rm DH} = \frac{q_\perp^2}{Q^2+q_\perp^2} W_{\rm TL}^{\rm DH} \tag{48}$$

$$W_{\Delta}^{\rm DH} = \sin\gamma_{\rm CS}\cos\gamma_{\rm CS} W_{\rm TL}^{\rm DH} = -\frac{Q q_\perp}{Q^2+q_\perp^2} W_{\rm TL}^{\rm DH} \tag{49}$$

$$W_{\Delta\Delta}^{\rm DH} = \tfrac{1}{2} W_L^{\rm DH}. \tag{50}$$

Immediately one observes that the Lam-Tung relation holds in the CS frame and all other frames considered here. For the Gottfried-Jackson frame the results get particularly simple. The double-hard contributions for deviations from the simple $1+\cos^2\theta$ behaviour vanish completely:

$$W_{\rm L}^{\rm DH} = 0\,, \quad W_{\Delta}^{\rm DH} = 0\,, \quad W_{\Delta\Delta}^{\rm DH} = 0\,. \tag{51}$$

At first glance this seems to be rather surprising but it is a direct consequence of the special form of all double-hard contributions and therefore has a simple explanation.

The double hard process resembles the classical double scattering picture. To understand this we consider again the process depicted in Fig. 1. The antiquark from the hadron undergoes a first scattering with a hard gluon from the nucleus. By subsequently radiating a gluon with large transverse momentum the antiquark returns to the mass shell, but now with transverse momentum $q_\perp$. The second scattering then corresponds to the lowest-order annihilation process of two massless quarks. Therefore the double-hard process can be factored as the product of two single scattering cross sections, supported by our model that the double-hard matrix element can in good approximation be written as a product of two twist 2 distribution functions. This process naturally fulfills the Lam-Tung relation and depends only on the structure function $W_{\rm TL} \sim W_\mu^\mu$. Other helicity amplitudes differ only by kinematical factors, i.e. can be obtained from $W_{\rm TL}$ in the Gottfried-Jackson frame by simple rotations. In this probabilistic picture scaling by $A^{4/3}$ appears to be very natural. The cross section of the first scattering obviously scales by the volume $\sim A$ of the nucleus. Afterwards the projectile parton travels further through the nucleus and has to penetrate the nuclear matter. The probability whether a second interaction takes place on the way to the boundary of the nucleus scales then by the nuclear radius $\sim A^{1/3}$.

4.3 Calculation of the soft-hard processes

For soft-hard scattering we have to keep $K_\perp$ in the expansion of the gluon momenta. The limit $K_\perp = 0$ would lead to $K = 0$ which gives no contribution to physical double scattering but just

a contribution of the eikonal phase. Note that we are always using covariant gauge where these factors are present. Starting from equation (31) we do a collinear expansion

$$\tilde{H} = \tilde{H}|_{\substack{K_\perp=0\\K'_\perp=0}} + K_\perp^\lambda \frac{\mathrm{d}}{\mathrm{d}K_\perp^\lambda}\tilde{H}|_{K_\perp=0} + \frac{1}{2!}K_\perp^\lambda K_\perp^\kappa \frac{\mathrm{d}^2}{\mathrm{d}K_\perp^\lambda\,\mathrm{d}K_\perp^\kappa}\tilde{H}|_{K_\perp=0} + \dots . \tag{52}$$

of the terms depending on intrinsic transverse momentum

$$\tilde{H} = \int \frac{\mathrm{d}x\,\mathrm{d}x'}{\xi_1} e^{ir_1^+ z_1^-} e^{iK^+ z_3^-} e^{-iK'^+ z_4^-} \bar{H}(\xi_1, \xi_2, x, x', K_\perp, K'_\perp). \tag{53}$$

We have used $K_\perp = K'_\perp$ which allows us to write

$$K_\perp^\lambda \frac{\mathrm{d}}{\mathrm{d}K_\perp^\lambda} = K_\perp^\lambda \frac{\partial}{\partial K_\perp^\lambda} + K'_\perp{}^\lambda \frac{\partial}{\partial K'_\perp{}^\lambda}. \tag{54}$$

The mixed terms of second order proportional to $K_\perp^\lambda K'_\perp{}^\kappa$ give the leading contribution to soft hard scattering. The factor $K_\perp^\lambda K'_\perp{}^\kappa$ can be converted into partial derivatives with respect to z_3^-, z_4^-. A partial integration and an expansion $A^\rho = A^+ P_1^\rho / P_1^+ + \dots$ for soft gluon fields in the nuclear matrix elements turns them into field strength tensors. The $K_\perp$ and $K'_\perp$ integrals can then be carried out. Note that having soft quarks with transverse momentum and converting the corresponding $K_\perp$ into covariant derivatives acting on the quark fields would lead to operators contributing only at the level of twist-6 [6].

We perform the pole integrations for the symmetrically cut graphs (M) in Figs.7 and the corresponding asymmetrically cut ones (R) and (L). The residues fix the momentum fractions of the soft gluons to $x = x_s = x'$ while the hard partons carry $\xi_1 = x_b$ for the symmetric diagrams and $\xi_1 = x_c$ for the asymmetric diagrams and

$$x_s = \frac{k_\perp^2}{\xi_2 S}, \tag{55}$$

$$x_b = \tilde{\xi}_b - x_s = -\frac{\xi_2(U-Q^2) + Q^2 - 2qK_\perp - k_\perp^2}{\xi_2 S + T - Q^2} - \frac{k_\perp^2}{\xi_2 S}, \tag{56}$$

$$x_c = \tilde{\xi}_c = -\frac{\xi_2(U-Q^2) + Q^2}{\xi_2 S + T - Q^2}. \tag{57}$$

We have introduced the notation $k_\perp^2 = -K_\perp^2 \geq 0$. When we take a forward diagram for soft-hard scattering then the sum of differently cut diagrams (M), (R) and (L) can be divided into two terms. This procedure is described in detail in [7, 8]. In the first term, phase factors and Θ-functions arrange in such a way that this term is bounded in space-time by geometrical arguments and cannot pick up an additional factor $A^{1/3}$. This contribution shows no nuclear enhancement. The second term is not bounded and only depends on the hard part of the symmetric diagram (M). We therefore neglect the first term and arrive at

$$W_\alpha^{\mathrm{SH}/ab+c} = (2\pi)^2 (4\pi\alpha_s)^2 e_q^2 \int_B^1 \frac{\mathrm{d}\xi_2}{\xi_2} \frac{1}{\xi_2 S + T - Q^2} f_{c/H}(\xi_2) \Big(-\frac{g^{\lambda\kappa}}{4}\Big) \frac{\mathrm{d}^2}{\mathrm{d}K_\perp^\lambda\,\mathrm{d}K_\perp^\kappa}\Big|_{K_\perp=0} T_{ab}^{\mathrm{SH}}(x_b) \frac{1}{x_b} H_\alpha^{\mathrm{SH},ab+c}(x_b, x_s, \xi_2) \tag{58}$$

where $\alpha \in \{\mu\nu, \mathrm{TL}, \mathrm{L}, \Delta, \Delta\Delta\}$. The hard part for the $qg + \bar{q}$ process shown in Fig. 7(a) is

$$H_{\mu\nu}^{\mathrm{SH}/qg+\bar{q}} = \mathcal{C} \frac{1}{(\xi_2 S)^2} \frac{1}{4} \,\mathrm{Tr}\,[R_{\nu\beta}(-\not{r}_2 - \not{K})\ \not{P}_1\ \not{r}_2\ \not{P}_1(-\not{r}_2 - \not{K}) L_{\alpha\mu}\gamma_\mu\ \not{r}_1\gamma_\nu]\ {}_{\substack{\xi_1=x_b\\x=x'=x_s}}\ (-g^{\alpha\beta}) \tag{59}$$

$L_{\alpha\mu}$ and $R_{\nu\beta}$ stand for the tree-level diagrams on the left- and the right-hand side of the diagram in Fig. 7(a) indicated by the blobs. $\mathcal{C}$ symbolizes the color factor of each single diagram. Hard parts for $qg+g$ and $gg+q$ subprocesses are obtained in an analogous fashion.

The universal matrix elements appearing for soft-hard scattering depend only on the momentum fraction x_b of the hard parton and are given by

$$\begin{aligned} T_{qg}^{\mathrm{SH}}(x_b) &= \frac{1}{2}\int \mathrm{d}z_4^- \frac{\mathrm{d}z_1^-}{2\pi}\frac{\mathrm{d}z_3^-}{2\pi}\Theta(z_1^- - z_3^-)\Theta(-z_4^-)e^{ix_bP_1^+z_1^-} \\ &\quad \langle P_1|\, F^{\omega+}(z_4^-)\bar{q}(0)\gamma^+ q(z_1^-)F^+{}_\omega(z_3^-)\,|P_1\rangle \\ T_{gg}^{\mathrm{SH}}(x_b) &= \frac{1}{x_bP_1^+}\int \mathrm{d}z_4^- \frac{\mathrm{d}z_1^-}{2\pi}\frac{\mathrm{d}z_3^-}{2\pi}\Theta(z_1^- - z_3^-)\Theta(-z_4^-)e^{ix_bP_1^+z_1^-} \\ &\quad \langle P_1|\, F^{\omega+}(z_4^-)F^+{}_\omega(z_3^-)F^{\lambda+}(0)F^+{}_\lambda(z_1^-)\,|P_1\rangle \end{aligned} \tag{60}$$

for scattering off a quark-gluon and a gluon-gluon pair in the nucleus, respectively. We can repeat the arguments given below eq. (44) for the nuclear enhancement. Since the longitudinal momentum fraction of the gluons is essentially zero, we even encounter only one phase factor $e^{ix_bP_1^+z_1^-}$ contrary to the case of double hard scattering discussed before. One therefore might expect that soft-hard matrix elements lead to an enhancement factor proportional to the square of the nuclear radius $A^{2/3}$ since only one out of three integrations is limited by phase factors. However, the fields at positions z_3^- and z_4^- are correlated by color forces. The anticipated absence of long-range color correlations in a nucleus implies that integration over $z_4^- - z_3^-$ is still restricted to a region of the size of a nucleon.

To build a model for the soft hard matrix elements one again can compare eq. (60) with the definition of the usual twist-2 matrix elements eq. (22). Neglecting for a moment the Θ-functions we see that the twist-4 pieces differ only by an additional x_b independent renormalization. Assuming that this can be factored into a term proportional to the nuclear radius and a (possibly scale dependent) constant λ^2

$$A^{1/3}\lambda^2 \sim \int \mathrm{d}z_4^- \frac{\mathrm{d}z_3^-}{2\pi} F^{\omega+}(z_4^-)F^+{}_\omega(z_3^-) \tag{61}$$

the x_b dependence of the twist-4 matrix element can be modeled by the usual twist-2 structure function.

$$T_{ab}^{\mathrm{SH}}(x) = \lambda^2 A^{\frac{4}{3}} f_{a/A}(x) \tag{62}$$

Eq. (61) can be interpreted as the collective color-magnetic Lorentz force experienced by the projectile parton while traveling through nuclear matter [6].

The only $K_\perp$-dependence of the hard part will be implicit in x_b and x_s. Therefore we can rewrite the derivatives in the form

$$\begin{aligned} W_\alpha^{\mathrm{SH},ab+c} =& (2\pi)^2(4\pi\alpha_s)^2 e_q^2 \int_B^1 \frac{\mathrm{d}\xi_2}{\xi_2}\frac{1}{\xi_2 S + T - Q^2} f_{c/H}(\xi_2) \\ & \frac{1}{2}\left[\frac{\partial^2}{\partial x_c^2}\left(T_{ab}^{\mathrm{SH}}(x_c)\frac{1}{x_c}H_\alpha^{\mathrm{SH},ab+c}(x_c,\xi_2)\right)\frac{2q_\perp^2}{(\xi_2 S+T-Q^2)^2} + \right. \\ & + \frac{\partial}{\partial x_c}\left(T_{ab}^{\mathrm{SH}}(x_c)\frac{1}{x_c}H_\alpha^{\mathrm{SH},ab+c}(x_c,\xi_2)\right)\frac{2(Q^2-T)}{\xi_2 S(\xi_2 S+T-Q^2)} + \\ & \left. + T_{ab}^{\mathrm{SH}}(x_c)\frac{1}{x_c}(H_\alpha^{\mathrm{SH},ab+c})'(x_c,\xi_2)\frac{2}{\xi_2 S}\right] \end{aligned} \tag{63}$$

where $H(x_c,\xi_2) = H(x_c, x_s = 0, \xi_2)$ and $H'(x_c,\xi_2) = \frac{\partial}{\partial x_s} H(x_c, x_s = 0, \xi_2)$. Note that in [8] the last term containing a derivative with respect to x_s is absent since it turns out that $H_{\rm TL}^{\rm SH}$ does not depend explicitly on x_s. We give the results for the hard parts in the Collins-Soper frame in Appendix 7.4. There are some subtleties in removing the unphysical degrees of freedom for processes of the class $qg + g$. There we have soft quarks from the nucleus with dominating component A^+ and for the hard gluons from the single hadron we have to take only the transverse polarizations. For $W_{\rm TL}^{\rm SH}$ we reproduce the results of [8]. Unlike for double-hard scattering the amplitudes $W_L^{\rm SH}$, $W_\Delta^{\rm SH}$ and $W_{\Delta\Delta}^{\rm SH}$ cannot be obtained in a trivial way from $W_{\rm TL}$. Related to that is an obvious violation of the Lam-Tung relation.

5 Numerical Results

In order to cover different energies S we calculated helicity amplitudes and angular coefficients for two different settings: for 252 GeV π^- on tungsten as in the Fermilab E615 experiment [19] and for future $p + A$ collider experiments at RHIC energies with 250 GeV protons and $A \times 100$ GeV large nuclei. The main task before doing the numerics is to insert a suitable model for the twist-4 matrix elements in the nucleus. The models introduced in the last sections for the double-hard matrix elements

$$T_{ab}^{\rm DH}(x_a, x_h) = C A^{\frac{4}{3}} f_{a/A}(x_a) f_{b/A}(x_h). \tag{64}$$

and for the soft-hard matrix elements

$$T_{ab}^{\rm SH}(x) = \lambda^2 A^{\frac{4}{3}} f_{a/A}(x) \tag{65}$$

are already given by LQS [7, 8]. We tried to argue above that their dependence on the parton momentum fractions and their scaling behaviour with respect to A seem to be quite natural.

Nevertheless the correct normalization of the models is not yet clear. The hope is that C and λ are universal constants. In the early days of the model a value of $C = 0.072$ GeV^2 was taken from theory [8, 24] while λ^2 was taken from comparison with experiment. This was done by analyzing dijet photoproduction on nuclei [6, 25] leading to a value $\lambda^2 = 0.05 - 0.1$ GeV^2. Later an analysis of $q_\perp$-broadening in hadron-nucleon Drell-Yan processes [9] implied a value of $\lambda^2 = 0.01$ GeV^2. Obviously there is a discrepancy, which may either point to a strong scale dependence or questions the universality of the soft-hard nuclear matrix elements. Note that the soft interaction besides the hard process in soft-hard double scattering is a final state interaction for dijet photoproduction but an initial state interaction for the Drell-Yan process.

In their latest work Guo, Qiu and Zhang [17] used the fact that there is a formal connection between soft-hard and double-hard matrix elements via the limit

$$\lim_{x_g \to 0} x_g T_{qg}^{\rm DH}(x_q, x_g) = T_{qg}^{\rm SH}(x_q) \tag{66}$$

which leads with the models of eqs. (64),(65) to

$$C \approx \frac{\lambda^2}{x_g g(x_g)|_{x_g \approx 0}}. \tag{67}$$

They take $x_g g(x_g)|_{x_g \approx 0} \approx 3$ as the gluon momentum density at $x_g \longrightarrow 0$. Taking into account the later value of λ^2 this leads to a normalization factor C which is an order of magnitude below the former theoretical value. But it is more consistent with the value of $C \approx 0.005$ GeV^2 which we obtained in section 4 from a naive normalization argument.

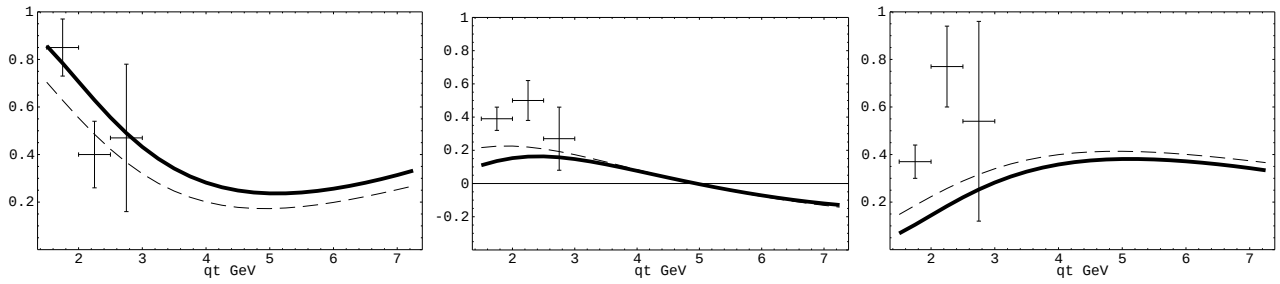

Figure 8: The angular coefficients λ, μ and ν (from left to right) as functions of $q_\perp$ in the Gottfried-Jackson frame for 252 GeV π^- on tungsten at $Q = 5$ GeV, $y = 0$. The dashed line is the result for single-scattering and the thick line is given by the full calculation with single- and double-scattering. We also show results of the E615 experiment at low transverse momentum.

In another, more geometrical, model one can estimate the two-parton area density that can be seen by the projectile parton in the nucleus by the product of two single-parton area densities. Integration of the two-parton area density over the effective transverse area of the nucleus yields exactly the right-hand side of eq. (64) with a constant $C = 9/(8\pi r_0^2) \approx 0.01$ GeV^2. Obviously C is presently basically unknown and a true improvement can only be expected if comparisons of a larger number of observables with more precise experimental data are available.

For soft-hard scattering we use the smaller value of $\lambda^2 = 0.01$ GeV^2 obtained from Drell-Yan data to maintain consistency. For double-hard scattering we have chosen the maximal value $C = 0.072$ GeV^2 to give a feeling how big the effects of double scattering might be. We take the twist-2 distribution functions from the CTEQ3M parameterization for the nucleons [27] and from the recent GRS fits for the pion [28]. Where nuclear effects on twist-2 distribution functions are taken into account the EKS98 parametrization [29] is used.

Let us first address the question how this approach works with the pion data from E615. In Fig. 8 we show our results for the angular coefficients λ, μ and ν in the Gottfried-Jackson frame for the process $\pi^- + W$ at E615 energy. We also give experimental data from the E615 collaboration. We can fairly well describe the data for λ at low transverse momentum but fail for μ and ν. It seems to be an essential feature that corrections due to nuclear enhanced twist-4 matrix elements can be quite large for the helicity amplitudes but the effects largely cancel for the angular coefficients which are ratios thereof. Therefore changes of the angular coefficients in the range $q_\perp \approx Q$ are small compared with the pure twist-2 calculation. Experimental values have

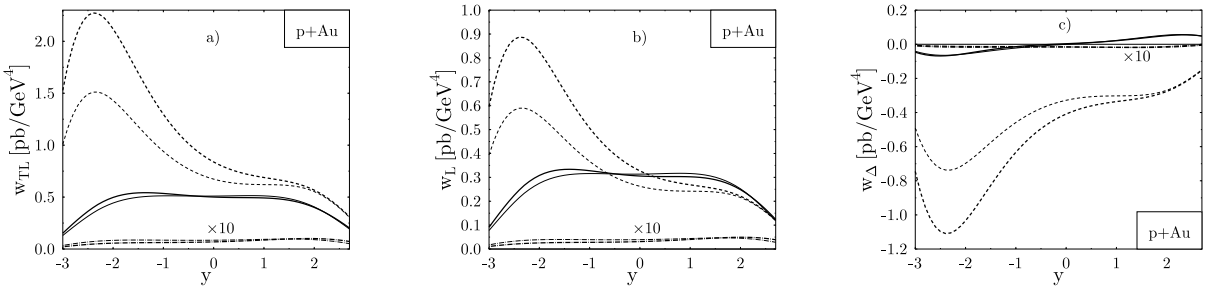

Figure 9: The helicity amplitudes $w_{\rm TL}$, $w_{\rm L}$ and w_Δ for $p + Au$ collisions at $S = 10^5$ GeV, $Q = 5$ GeV and $q_\perp = 4$ GeV. We show the twist-2 contribution (solid lines), double-hard (dashed lines), and soft-hard (dashed-dotted lines). Soft-hard is scaled up by a factor of 10. We give results with (thin lines) and without (thick lines) EKS98 modifications for nuclear parton distributions.

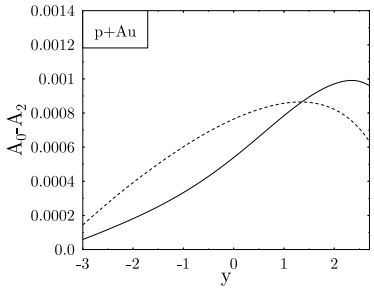

Figure 10: Violation of the Lam-Tung relation. Difference of angular coefficients A_0 and A_2 is shown. Calculation are with (solid line) and without (dashed line) EKS98 corrections to nuclear parton distributions.

large error bars above $q_\perp = 2$ GeV. We already pointed out that data at $q_\perp/Q \approx 1$ would provide a much better test for the twist-4 calculation because of the absence of soft-hard interference terms and the absence of double logarithmic corrections of the type $\log^2(Q^2/q_\perp^2)$ which have to be resummed. We have to conclude that nuclear enhanced double scattering contributions are not able to yield substantial improvement for the old pion data. Deviations of the $\pi - W$ data from the naive perturbative QCD-predictions might be explained by other approaches like the Berger-Brodsky mechanism which takes into account higher twist contributions of the pion wave function [30], in terms of non-trivial spin correlations in the QCD-vacuum [31] or via contributions of the chiral-odd T-odd distribution function $h_1^\perp$ [32].

We turn to $p + Au$ collisions at RHIC with $S = 10^5$ GeV^2 per nucleon pair. We give helicity amplitudes instead of angular coefficients since these provide a clearer measure of nuclear enhanced higher twist effects as explained above. To make numerical results of helicity amplitudes W_α, $\alpha \in \{\mathrm{TL}, \mathrm{L}, \Delta, \Delta\Delta\}$ more meaningful, we introduce the prefactor given in eq. (13),

$$w_\alpha = \frac{\alpha^2}{64\pi^3 S Q^2} W_\alpha, \tag{68}$$

to convert the quantities W_α into differential cross sections. In Fig. 9 we give single scattering, double-hard and soft-hard results for the helicity amplitudes w_{TL}, w_{TL} and w_Δ as functions of rapidity y in the Collins-Soper frame. One can read off the main results already given in [10]. First the nuclear enhanced twist-4 contribution is absolutely important at RHIC energies. Even at quite large values of $Q = 5$ GeV and $q_\perp = 4$ GeV used for the calculation its effect can exceed the leading-twist result for the parameters used. Second the double-hard contribution is by far

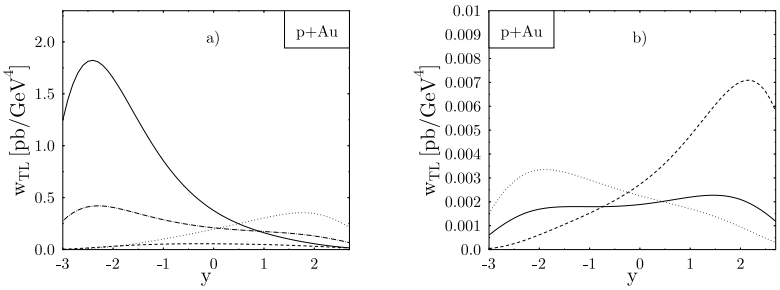

Figure 11: Contributions of different subprocesses to w_{TL} for double-hard (a) and soft-hard (b) scattering. Double-hard subprocesses are $qg + \bar{q}$ (solid line), $qg + g$ (dashed line), $q\bar{q} + g$ (dotted line) and $q\bar{q} + q$ plus all pure fermionic processes (dash-dotted line). Soft-hard processes are $qg + \bar{q}$ (solid line), $qg + g$ (dashed line) and $gg + q$ (dotted line).

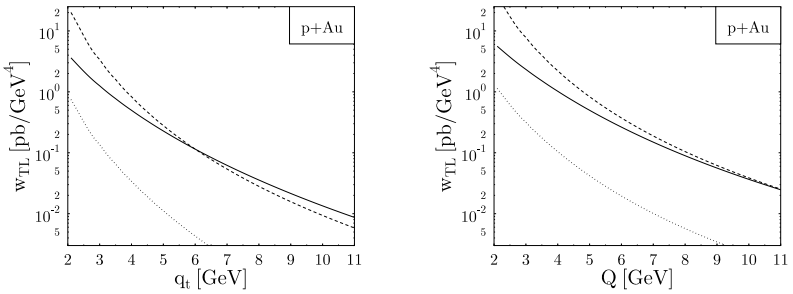

Figure 12: $w_{\rm TL}$ as a function of transverse momentum $q_\perp$ at fixed $Q = 5$ GeV, $y = 0$ (left) and as a function of photon mass Q at $q_\perp = 4$ GeV and $y = 0$ (right). Curves are shown for single scattering (solid line), double-hard (dashed line) and soft-hard scattering (dotted line).

larger than the soft-hard part in the kinematical range under consideration. This can be seen for all helicity amplitudes in Fig. 9. Even if we use smaller values of C proposed above double-hard scattering would reach the same order of magnitude as single scattering.

We also give results with EKS98 modifications to nuclear parton distributions. These parametrizations take into account shadowing, antishadowing and other nuclear effects on parton distributions, first described by the European Muon Collaboration. The numerical effect of these modifications on the single scattering results are small, but they turn out to be quite large for double-hard scattering. Note that it is not clear whether these nuclear effects for twist-2 parton distributions should be carried over to the models for twist-4 matrix elements. We give results for modified and unmodified distributions to indicate the further uncertainty of the twist-4 matrix elements. The sensitivity of double-hard scattering to these EKS98 modifications is simply related to the fact that they involve a product of two nuclear parton distributions. The general question about the correct small-x behaviour of the twist-4 nuclear matrix elements is very interesting since it has a big influence at RHIC energies.

We return to the question of the Lam-Tung relation. We already saw analytically that double-hard scattering respects this relation while soft-hard does not. In Fig. 10 we show the difference $A_0 - A_2$. It only picks up contributions from soft-hard scattering and therefore this quantity is very small. That means that violation of the Lam-Tung sum rule is a tiny effect for the process under consideration.

The characteristic feature of the rapidity distribution is the peak of the double-hard distribution at negative rapidities (i.e. for the photon emitted in direction of the initial single hadron). The reason for this is that negative rapidity prefers small Bjorken-x for partons from the nucleus. Parton distributions at small parton momentum fractions are large particularly for gluons and they enter quadratically for double-hard scattering. In Fig. 11 we separated the different partonic subprocesses contributing to double-hard and soft-hard scattering to enable a deeper analysis. One can see that double-hard processes with a quark and a gluon from the nucleus dominate over those with two quarks at negative rapidities (i.e. small x_h). On the other hand $qg + \bar{q}$ is more important than $qg + g$ in this region since momentum fraction ξ_2 of the parton from the single hadron is large and quarks dominate over gluons in that case. All the rapidity spectra can be understood in this way.

Fig. 12 shows dependence of $w_{\rm TL}$ on photon mass Q and transverse momentum $q_\perp$. It can be seen that soft-hard and double-hard contributions as expected for higher-twist processes fall off more rapidly with Q and $q_\perp$ than (twist-2) single-scattering.

6 Summary

We have calculated nuclear enhanced double-scattering contributions to Drell-Yan pair production in hadron-nucleus collisions using the framework of Luo, Qiu and Sterman. We found that the nuclear enhancement at RHIC energies and large transverse momentum makes double scattering a contribution that is equally important as single scattering. Measurements of angular coefficients and helicity amplitudes can distinguish double-hard and soft-hard scattering. Double-hard scattering has the interpretation of two sequential hard scatterings of onshell partons and is therefore related to probabilistic pictures of multiple scattering that are widely used in the phenomenology of heavy-ion reactions. In this spirit further comparision with alternative approaches to multiple scattering [5, 34] would be very interesting.

Double-hard scattering respects the Lam-Tung relation and, in contrast to soft-hard scattering, does not show non-trivial deviations from the $1 + \cos^2\theta$ angular distribution. Numerically double-hard scattering dominates over the soft-hard contribution. Soft-hard scattering violates the Lam-Tung relation but this violation is an effect of order 10^{-3} for the model used.

Double-hard scattering can be modeled as the product of two twist-2 structure functions which give the probability for finding two partons in the nucleus. The soft-hard matrix elements on the other hand encodes essential non-perturbative properties of the nucleus, describing the influence of the collective color field on the transverse momentum of the produced lepton pair. Inserting reasonable models for the corresponding matrix elements we predict, that collective color effects are negligible compared to the effects of subsequent independent hard scatterings in the kinematical range considered here. However the absolute normalization of the twist-4 matrix elements in these models is not yet clear.

The double-hard scattering shows an interesting asymmetry in the rapidity distribution of the Drell-Yan pair. The pair is predominantly produced in the projectile, i.e. single hadron rapidity region. Although the absolute counting rates for the DY pairs at large transverse momentum are not high [10] the predicted effect fits perfectly well in the PHENIX detector acceptance [33]. This asymmetry therefore should be observable.

An analysis of W_L and W_Δ, particularly in the Gottfried-Jackson frame, as well as the measurement of $W_{\rm TL}$ (i.e. the angular integrated cross section) as a function of rapidity can check whether double-hard scattering is the dominant contribution. A possible violation of the Lam-Tung sum rule provides a further possibility to check the picture of soft-hard and double-hard scattering in general. If our predictions with respect to the ratio of soft-hard and double-hard scattering are confirmed by experiment it would provide support for the description of heavy ion reactions in terms of incoherent multiple scattering of free partons. Note that the prediction of a trivial frame dependence of double-hard scattering and the conservation of the Lam-Tung relation are independent of the models for the twist-4 distribution functions and provide good tests for the entire LQS approach.

Acknowledgements. We are grateful to X. Guo for helpful correspondence. In course of the work we benefitted from discussions with V. Braun, L. Syzmanowsky, and O. Teryaev. E. S. thanks G. Sterman and X.N. Wang for useful discussions.

7 Appendix

7.1 Transformation of amplitudes to different frames

Here we list the matrices $M_{(\beta)}$ defined in eq. (20) that map the invariant projections of the hadronic tensor to the set of helicity amplitudes ($W_{\rm TL}$, W_L, W_Δ, $W_{\Delta\Delta}$). They are

$$
\begin{aligned}
M_{\rm CS} &= \begin{pmatrix}
\frac{1}{2} & 0 & 0 & 0 \\
0 & \frac{1}{4\cos^2\gamma_{\rm CS}} & \frac{1}{4\cos^2\gamma_{\rm CS}} & -\frac{1}{4\cos^2\gamma_{\rm CS}} \\
0 & -\frac{1}{4\sin\gamma_{\rm CS}\cos\gamma_{\rm CS}} & \frac{1}{4\sin\gamma_{\rm CS}\cos\gamma_{\rm CS}} & 0 \\
\frac{1}{2} & -\frac{1+\cos^2\gamma_{\rm CS}}{8\cos^2\gamma_{\rm CS}\sin^2\gamma_{\rm CS}} & -\frac{1+\cos^2\gamma_{\rm CS}}{8\cos^2\gamma_{\rm CS}\sin^2\gamma_{\rm CS}} & \frac{1-3\cos^2\gamma_{\rm CS}}{8\cos^2\gamma_{\rm CS}\sin^2\gamma_{\rm CS}}
\end{pmatrix} \\
M_{\rm GJ} &= \begin{pmatrix}
\frac{1}{2} & 0 & 0 & 0 \\
0 & 1 & 0 & 0 \\
0 & -\cot\gamma_{\rm GJ} & 0 & -\frac{1}{2\sin\gamma_{\rm GJ}} \\
\frac{1}{2} & -\frac{1+\cos^2\gamma_{\rm GJ}}{2\sin^2\gamma_{\rm GJ}} & -\frac{1}{\sin^2\gamma_{\rm GJ}} & \frac{\cos\gamma_{\rm GJ}}{\sin^2\gamma_{\rm GJ}}
\end{pmatrix}
\end{aligned}
\tag{69}
$$

for the Collins-Soper and the Gottfried-Jackson frame, respectively. $\gamma_{\rm CS}$ denotes the angle between $\mathbf{P}_1$ and the $\mathbf{Z}$ axis in the photon rest frame and $\gamma_{\rm GJ}$ is the angle between $\mathbf{P}_1$ and $\mathbf{P}_2$. Obviously $2\gamma_{\rm CS} + \gamma_{\rm GJ} = \pi$ and in terms of hadronic Mandelstam variables we have

$$
\begin{aligned}
\cos\gamma_{\rm CS} &= \sqrt{\frac{Q^2 S}{(Q^2-T)(Q^2-U)}}, \qquad & \sin\gamma_{\rm CS} &= -\sqrt{1-\frac{Q^2 S}{(Q^2-T)(Q^2-U)}} \\
\cos\gamma_{\rm GJ} &= 1-\frac{2Q^2 S}{(Q^2-T)(Q^2-U)}, \qquad & \sin\gamma_{\rm GJ} &= \frac{2Q^2 S}{(Q^2-T)(Q^2-U)}\sqrt{\frac{(Q^2-T)(Q^2-U)}{Q^2 S}-1}.
\end{aligned}
\tag{70}
$$

7.2 Single-scattering results

Here we list the results for the hard parts H_α of single-scattering helicity amplitudes in the Collins-Soper frame. They are defined in eq. (26). We distinguish annihilation and Compton processes.

$$
\begin{aligned}
H_{\mathrm{TL}}^{q+\bar{q}} &= \mathcal{C}_1 \frac{1}{tu}\left((Q^2-t)^2+(Q^2-u)^2\right)\\
H_{\mathrm{L}}^{q+\bar{q}} &= \mathcal{C}_1\left(\frac{Q^2-t}{Q^2-u}+\frac{Q^2-u}{Q^2-t}\right)\\
H_{\Delta}^{q+\bar{q}} &= \mathcal{C}_1\sqrt{\frac{Q^2 s}{tu}}\left(\frac{Q^2-u}{Q^2-t}-\frac{Q^2-t}{Q^2-u}\right)\\
H_{\Delta\Delta}^{q+\bar{q}} &= \frac{1}{2}H_L^{q+\bar{q}}\\
H_{\mathrm{TL}}^{q+g} &= -\mathcal{C}_2\frac{(Q^2-s)^2+(Q^2-t)^2}{st}\\
H_{\mathrm{L}}^{q+g} &= -\mathcal{C}_2\frac{u}{s}\frac{(Q^2+s)^2+(Q^2-t)^2}{(Q^2-t)(Q^2-u)}\\
H_{\Delta}^{q+g} &= -\mathcal{C}_2\sqrt{\frac{Q^2 u}{st}}\frac{2(Q^2-t)^2-(Q^2-u)^2}{(Q^2-t)(Q^2-u)}\\
H_{\Delta\Delta}^{q+g} &= \frac{1}{2}H_L^{q+g}\\
H_{\mathrm{TL}}^{g+q} &= -\mathcal{C}_2\frac{(Q^2-s)^2+(Q^2-u)^2}{su}\\
H_{\mathrm{L}}^{g+q} &= -\mathcal{C}_2\frac{t}{s}\frac{(Q^2+s)^2+(Q^2-u)^2}{(Q^2-t)(Q^2-u)}\\
H_{\Delta}^{g+q} &= \mathcal{C}_2\sqrt{\frac{Q^2 t}{su}}\frac{2(Q^2-u)^2-(Q^2-t)^2}{(Q^2-t)(Q^2-u)}\\
H_{\Delta\Delta}^{g+q} &= \frac{1}{2}H_L^{g+q}.
\end{aligned}
\tag{71}
$$

$\mathcal{C}_1 = C_F/N_c = 4/9$ and $\mathcal{C}_2 = 1/(2N_c) = 1/6$ are essentially the color factors.

7.3 Double-hard results

In this section we give the hard parts $H_{\rm TL}$ of the projections $W_{\rm TL}^{\rm DH}$ for double-hard processes. They do not depend on the frame.

$$
\begin{aligned}
H_{\rm TL}^{DH,qg+\bar{q}} &= \frac{2}{27}\left(\frac{(Q^2-T)}{\xi_2 S}+\frac{\xi_2 S}{Q^2-T}\right)+\frac{1}{6}\frac{(Q^2-T)^2+(\xi_2 S)^2}{\xi_2 S+T-Q^2}\\
H_{\rm TL}^{DH,qg+g} &= \frac{1}{36}\left(\frac{\xi_2 S+T-Q^2}{Q^2-T}+\frac{Q^2-T}{\xi_2 S+T-Q^2}\right)-\frac{1}{16}\frac{(Q^2-T)^2+(\xi_2 S+T-Q^2)^2}{(\xi_2 S)^2}\\
H_{\rm TL}^{DH,q\bar{q}+g} &= \frac{2}{27}\left(\frac{\xi_2 S+T-Q^2}{\xi_2 S}+\frac{\xi_2 S}{\xi_2 S+T-Q^2}\right)+\frac{1}{6}\frac{(\xi_2 S)^2+(\xi_2 S+T-Q^2)^2}{(Q^2-T)^2}\\
H_{\rm TL}^{DH,q\bar{q}+q} &= \frac{2}{27}\left(\frac{(\xi_2 S)^2+(\xi_2 S+T-Q^2)^2}{(Q^2-T)^2}+\frac{(Q^2-T)^2+(\xi_2 S+T-Q^2)^2}{(\xi_2 S)^2}\right)+\\
&\quad+\frac{4}{81}\frac{(\xi_2 S+T-Q^2)^2}{\xi_2 S(Q^2-T)}\\
H_{\rm TL}^{DH,q\bar{q}+\bar{q}} &= \frac{2}{27}\left(\frac{(\xi_2 S)^2+(\xi_2 S+T-Q^2)^2}{(Q^2-T)^2}+\frac{(Q^2-T)^2+(\xi_2 S)^2}{(\xi_2 S+T-Q^2)^2}\right)-\\
&\quad-\frac{4}{81}\frac{(\xi_2 S)^2}{(Q^2-T)(\xi_2 S+T-Q^2)}\\
H_{\rm TL}^{DH,qq+\bar{q}} &= \frac{2}{27}\left(\frac{(Q^2-T)^2+(\xi_2 S+T-Q^2)^2}{(Q^2-T)^2}+\frac{(Q^2-T)^2+(\xi_2 S)^2}{(\xi_2 S+T-Q^2)^2}\right)+\\
&\quad+\frac{4}{81}\frac{(Q^2-T)^2}{\xi_2 S(\xi_2 S+T-Q^2)}\\
H_{\rm TL}^{DH,q\bar{q}+q'} &= \frac{2}{27}\frac{(\xi_2 S)^2+(\xi_2 S+T-Q^2)^2}{(Q^2-T)^2}\\
H_{\rm TL}^{DH,qq'+\bar{q}'} &= \frac{2}{27}\frac{(Q^2-T)^2+(\xi_2 S+T-Q^2)^2}{(\xi_2 S)^2}\\
H_{\rm TL}^{DH,qq'+\bar{q}} &= \frac{2}{27}\frac{(Q^2-T)^2+(\xi_2 S)^2}{(\xi_2 S+T-Q^2)^2}
\end{aligned}
\tag{72}
$$

7.4 Soft-hard results

Here we list the hard parts $H(T_\alpha)$ of the invariant projections $T_{\rm TL}^{\rm SH}$, $T_{\rm L1}^{\rm SH}$, $T_{\rm L2}^{\rm SH}$ and $T_{\rm L12}^{\rm SH}$ of the hadronic tensor, defined in section 2.2, for soft-hard processes. The results can be projected into a specific frame via eq. (20) and the matrices given in Appendix 7.1. This is mathematically trivial but it complicates the expressions substantially. For this reason we give only the invariant

projections. Note that especially $H_{\mathrm{TL}} = H(T_{\mathrm{TL}})/2$ for every frame described in section 2.2.

$$H(T_{\mathrm{TL}}^{qg+\bar{q}}) = \frac{4}{27}\left(\frac{(Q^2-T)(x_c-x_a)}{x_c(\xi_2 S+T-Q^2)} + \frac{2x_a\xi_2 S}{(x_c-x_a)(\xi_2 S+T-Q^2)} + \frac{x_c(\xi_2 S+T-Q^2)}{(Q^2-T)(x_c-x_a)}\right)$$

$$H(T_{\mathrm{L1}}^{qg+\bar{q}}) = \frac{8}{27}\frac{x_a\xi_2 S}{x_c(Q^2-T)}$$

$$H(T_{\mathrm{L2}}^{qg+\bar{q}}) = \frac{8}{27}\left(\frac{\xi_2 S+T-Q^2}{(x_c+x_s)S+U-Q^2}\frac{x_s Q^2 S}{(Q^2-U)^2} - \frac{x_a}{x_a-x_c}\frac{x_c S((x_c+x_s)S+U-Q^2)}{(Q^2-U)^2}\right.$$
$$\left. -\frac{x_a}{x_a-x_c}\frac{S^2}{(Q^2-U)^2}\frac{(x_c+x_s)((x_c-x_s)(Q^2-T)+\xi_2(Q^2-U)-x_c\xi_2 S)-(x_c-x_s)Q^2}{\xi_2 S+T-Q^2}\right)$$

$$H(T_{\mathrm{L12}}^{qg+\bar{q}}) = -\frac{8}{27}\left(\frac{x_a}{x_a-x_c}\frac{\xi_2 S^2}{(Q^2-T)(Q^2-T)}\frac{(x_c-x_s)(Q^2-T)+\xi_2(Q^2-U)-Q^2-x_c\xi_2 S}{\xi_2 S+T-Q^2}+\right.$$
$$\left. +\frac{x_a s}{x_c(Q^2-U)}\frac{(x_c+x_s)(\xi_2 S+T-Q^2)+\xi_2((x_c+x_s)S+U-Q^2)-Q^2+x_c\xi_2 S}{\xi_2 S+T-Q^2}\right)$$

$$H(T_{\mathrm{TL}}^{qg+g}) = \frac{1}{8}\left(\frac{x_c\xi_2 S}{(x_c-x_a)(Q^2-T)} - \frac{2x_a(\xi_2 S+T-Q^2)}{\xi_2 S(x_c-x_a)} + \frac{(x_c-x_a)(Q^2-T)}{x_c\xi_2 S}\right)$$

$$H(T_{\mathrm{L1}}^{qg+g}) = \frac{1}{4}\frac{x_a(\xi_2 S+T-Q^2)}{x_c(Q^2-T)}$$

$$H(T_{\mathrm{L2}}^{qg+g}) = \frac{1}{4}\left(\frac{x_s Q^2}{x_c(Q^2-U)}\frac{(x_c+x_s)S+U-Q^2}{\xi_2(Q^2-U)}-\right.$$
$$-\frac{x_a}{x_a-x_c}\frac{(x_c+x_s)S+U-Q^2}{\xi_2(Q^2-U)}\frac{(x_c-x_s)(Q^2-T)+\xi_2(Q^2-U)-Q^2-x_c\xi_2 S}{Q^2-U}-$$
$$\left.-\frac{x_a x_c}{x_a-x_c}\frac{((x_c+x_s)S+U-Q^2)(\xi_2 S+T-Q^2)+(Q^2-T)(Q^2-U)-Q^2 S}{\xi_2(Q^2-U)^2}\right)$$

$$H(T_{\mathrm{L12}}^{qg+g}) = \frac{1}{4}\left(\frac{x_a}{x_a-x_c}\frac{\xi_2 S+T-Q^2}{Q^2-T)}\frac{(x_c+x_s)(Q^2-T)-\xi_2(Q^2-U)-Q^2+x_c\xi_2 S}{\xi_2(Q^2-U)}+\right.$$
$$\left.+\frac{x_a}{x_c}\frac{(x_c+x_s)(\xi_2 S+T-Q^2)+\xi_2((x_c+x_s)S+U-Q^2)+Q^2-x_c\xi_2 S}{\xi_2(Q^2-U)}\right)$$

$$H(T_{\mathrm{TL}}^{qg+g}) = \frac{1}{18}\left(\frac{\xi_2 S}{\xi_2 S+T-Q^2} - \frac{2Q^2(Q^2-T)(x_c-x_a)}{x_c^2\xi_2 S(\xi_2 S+T-Q^2)}\frac{\xi_2 S+T-Q^2}{\xi_2 S}\right)$$

$$H(T_{\mathrm{L}}^{qg+g}) = -\frac{2}{9}\frac{x_a*(x_a-x_c)}{x_c^2}$$

$$H(T_{\Delta}^{qg+g}) = \frac{1}{9}\frac{Q^2}{Q^2-U}\left(\frac{(x_c+x_s)S+U-Q^2}{\xi_2(Q^2-U)} + \frac{x_s S}{(Q^2-U)}\frac{S}{\xi_2 S+T-Q^2}-\right.$$
$$-\frac{(x_c S+U-Q^2)((x_c+x_s)(\xi_2 S+T-Q^2)+\xi_2((x_c+x_s)S+U-Q^2)+Q^2-x_c\xi_2 S)}{x_c\xi_2(Q^2-U)(\xi_2 S+T-Q^2)}-$$
$$\left.\frac{2x_s Q^2((x_c+x_s)S+U-Q^2)}{x_c^2\xi_2(Q^2-U)(\xi_2 S+T-Q^2)}\right)$$

$$H(T_{\Delta\Delta}^{qg+g}) = -\frac{1}{9}\frac{x_a}{\xi_2 x_c}\left(\frac{2x_c\xi_2(Q^2-U)+x_c(x_c+x_s)(Q^2-T)+x_c^2\xi_2 S+2x_2 Q^2}{Q^2-U}+\right.$$
$$\left.+\frac{\xi_2((x_c+x_s)S+U-Q^2)(2Q^2+x_c(Q^2-T))+3x_c Q^2(Q^2-T)+2Q^4+x_c^2\xi_2^2 S^2}{(Q^2-U)(\xi_2 S+T-Q^2)}\right)$$

References

[1] J. C. Collins, D. E. Soper and G. Sterman,in *Perturbative Quantum Chromodynamics*, ed. A.H. Mueller (World Scientific, Singapore, 1989) and references therein.

[2] M. Arneodo, Phys. Rept. **240**, 301 (1994).

[3] J.P. Boymond *et al.*, Phys. Rev. Lett. **33**, 112 (1974); J.W. Cronin *et al.*, Phys. Rev. **D 11**, 3105 (1975).

[4] D.M. Alde *et al.*, Phys. Rev. Lett. **64**, 2479 (1990).

[5] G.T. Bodwin, S.J. Brodsky and G.P. Lepage, Phys. Rev. **D 39**, 3287 (1989); R. Baier, Y. L. Dokshitzer, A. H. Mueller, S. Peigne, and D. Schiff, Nucl. Phys. **B 484**, 265 (1997)

[6] M. Luo, J. Qiu and G. Sterman, Phys. Rev. **D 49**, 4493 (1994).

[7] M. Luo, J.W. Qiu and G. Sterman, Phys. Rev. **D 50**, 1951 (1994).

[8] X. Guo, Phys. Rev. **D 58**, 036001 (1998).

[9] X. Guo, Phys. Rev. **D 58**, 114033 (1998).

[10] R. J. Fries, B. Müller, A. Schäfer and E. Stein, Phys. Rev. Lett. **83**, 4261 (1999).

[11] S. A. Bass, B. Müller, and W. Pöschl, J. Phys. **G 25**, 109 (1999).

[12] C.S. Lam and W. Tung, Phys. Rev. **D 21**, 2712 (1980).

[13] K.J. Eskola, K. Kajantie, and J. Lindfors, Phys. Lett. **B 214**, 613 (1988).

[14] K. Geiger and B. Müller, Nucl. Phys. **B 369**, 600 (1992).

[15] K. Geiger, Phys. Rept. **258**, 237 (1995).

[16] L. McLerran and R. Venugopalan, Phys. Rev. **D 49**, 2233 and 3352 (1994).

[17] X. Guo, J. Qiu and X. Zhang, Eprint hep-ph/9911476 and Eprint hep-ph/9912361.

[18] S. Falciano *et al.*[NA10 Collaboration], Z. Phys. **C 31**, 513 (1986).

[19] J.S. Conway *et al.*, Phys. Rev. **D 39**, 92 (1989).

[20] C.S. Lam and W. Tung, Phys. Rev. **D 18**, 2447 (1978).

[21] J.C. Collins and D.E. Soper, Phys. Rev. **D 16**, 2219 (1977).

[22] E. Mirkes, Nucl. Phys. **B 387**, 3 (1992).

[23] J. Cleymans and M. Kuroda, Nucl. Phys. **B 155**, 480 (1979).

[24] A.H. Mueller and J. Qiu, Nucl. Phys. **B 268**, 427 (1986).

[25] D. Naples *et al.* [E683 Collaboration], Phys. Rev. Lett. **72**, 2341 (1994).

[26] M.A. Vasilev *et al.* [FNAL E866 Collaboration], Phys. Rev. Lett. **83**, 2304 (1999).

[27] H.L. Lai *et al.*, Phys. Rev. **D 51**, 4763 (1995).

[28] M. Glück, E. Reya and I. Schienbein, Eur. Phys. J. **C 10**, 313 (1999).

[29] K.J. Eskola, V.J. Kolhinen and C.A. Salgado, Eur. Phys. J. **C 9**, 61 (1999).

[30] A. Brandenburg, S. J. Brodsky, V. V. Khoze and D. Müller, Phys.Rev.Lett. **73**, 939 (1994); K.J. Eskola, P. Hoyer, M. Vanttinen and R. Vogt, Phys. Lett. **B 333**, 526 (1994).

[31] A. Brandenburg, O. Nachtmann and E. Mirkes, Z. Phys. **C 60**, 697 (1993).

[32] D. Boer, Phys.Rev. **D 60**, 014012 (1999)

[33] S. R. Tonse and J. H. Thomas, in: *Pre-Equilibrium Parton Dynamics*, ed. X.-N. Wang, Lawrence Berkeley Laboratory Report No. LBL-34831, p. 341 (1993).

[34] B.Z. Kopeliovich, A.V. Tarasov and A. Schäfer, Phys. Rev. **C 59**, 1609 (1999) ; B.Z. Kopeliovich, A.V. Tarasov and A. Schäfer, hep-ph/9908245; U.A. Wiedemann and M. Gyulassy, Nucl.Phys. **B 560**, 345 (1999)